

0686

NACA TN 3603

0066509



TECH LIBRARY KAFB, NM

NATIONAL ADVISORY COMMITTEE FOR AERONAUTICS

TECHNICAL NOTE 3603

THEORETICAL STUDY OF THE LATERAL FREQUENCY RESPONSE TO
GUSTS OF A FIGHTER AIRPLANE, BOTH WITH CONTROLS
FIXED AND WITH SEVERAL TYPES OF AUTOPILOTS

By James J. Adams and Charles W. Mathews

Langley Aeronautical Laboratory
Langley Field, Va.



Washington
March 1956

AMSC
TECHNICAL LIBRARY
TEL 631



TECHNICAL NOTE 3603

THEORETICAL STUDY OF THE LATERAL FREQUENCY RESPONSE TO

GUSTS OF A FIGHTER AIRPLANE, BOTH WITH CONTROLS

FIXED AND WITH SEVERAL TYPES OF AUTOPILOTS

By James J. Adams and Charles W. Mathews

SUMMARY

A theoretical approach has been used to determine the lateral frequency response of a fighter airplane to side gusts and to rolling gusts at a Mach number of 0.7 and an altitude of 30,000 feet. The frequency response and the power spectral density of the motion of the airplane in response to gusts were determined for the airplane with controls fixed and for the airplane in combination with three different basic types of attitude autopilots.

The response to gust inputs for the airplane with controls fixed exhibited a large resonance associated with the Dutch roll mode of the airplane. When the airplane was combined with the various autopilots, the addition of yaw damping greatly reduced the resonance. The addition of autopilot components to supply heading stability and roll stability provided good regulation in that the yaw and roll responses to gusts of the airplane were greatly reduced. Autopilots that controlled side force to low values and that provided good course response to command signals resulted in large roll response to side gusts.

A simplified transfer-function method of analysis for determining the response of the airplane-autopilot combinations was tried, and a comparison of the results of this method and the complete, three-degree-of-freedom method of analysis is given. It appears that the simplified method could be used for gust studies.

INTRODUCTION

One of the factors that affects the precision of such flight operations as landing and air gunnery is the response of the airplane to gust disturbances. Therefore, it is highly desirable to study the motions of airplanes and airplane-autopilot combinations which result from gusts and to establish which configurations are best suited to minimize the motions.

The present paper is concerned with the theoretical lateral frequency response and the power spectral density of the motion in response to gusts of a fighter airplane both with controls fixed and with three different types of attitude autopilots. The purpose of the paper can be stated as:

- (1) The development of equations expressing airplane lateral frequency response to gusts. The method used follows that developed in reference 1 which describes the longitudinal response to gusts.
- (2) The examination of the lateral frequency response to gusts and the power spectral density of the lateral response to atmospheric turbulence in an attempt to evaluate the relative merit of the autopilots in controlling the airplane.
- (3) The investigation of various simplified transfer-function methods of determining the response to gusts of the airplane-autopilot combination and the establishment of their merit.

The results are presented as plots of the frequency response and power spectral density of the motion of the airplane, both with controls fixed and in combination with the autopilots, in response to side-gust and rolling-gust inputs.

SYMBOLS

b	wing span, ft
C_L	lift coefficient, $\frac{L}{\frac{1}{2}\rho SV^2}$
C_l	rolling-moment coefficient, $\frac{L'}{\frac{1}{2}\rho SV^2 b}$
C_n	yawing-moment coefficient, $\frac{N}{\frac{1}{2}\rho SV^2 b}$
C_Y	side-force coefficient, $\frac{Y}{\frac{1}{2}\rho SV^2}$
D	differential operator, d/ds
g	acceleration due to gravity, ft/sec ²

K	autopilot gain
K_X	nondimensional radius of gyration about X-axis, k_X/b
K_Z	nondimensional radius of gyration about Z-axis, k_Z/b
K_{XZ}	nondimensional product-of-inertia factor
k_X	radius of gyration of airplane about X-axis, ft
k_Z	radius of gyration of airplane about Z-axis, ft
L	lift, lb
L'	rolling moment, ft-lb
l_x	nondimensional tail length parallel to X-axis, based on wing span
l_z	nondimensional distance (parallel to Z-axis) measured from X-axis to center of area of vertical tail
m	mass of airplane, slugs
N	yawing moment, ft-lb
n	frequency, cycles/sec
p	rolling angular velocity, radians/sec
r	yawing angular velocity, radians/sec
S	wing area, sq ft
s	distance measured in spans, tV/b
t	time, sec
V	velocity of airplane with respect to still air, ft/sec
v	velocity along Y-axis with respect to still air, ft/sec
v_g	velocity of side gust (positive gust produces sideslip to right), ft/sec
Y	side force, lb

α	angle of attack, radians
β	total sideslip angle, $\beta_0 + \beta_g$, radians
β_0	angle between X-axis and velocity vector V , radians
β_g	angle of sideslip due to side gust, radians
δ_a	total aileron angle, radians
δ_r	rudder angle, radians
κ	course, radians
μ	relative-density factor, $m/\rho S b$
ρ	air density, slugs/cu ft
σ	sidewash angle, radians
ϕ	angle of roll, radians
$D\phi_g$	nondimensional rolling gust, radians/span
ψ	heading or yaw angle, radians
ω	nondimensional circular frequency, $2\pi nb/V$, radians/span

Subscripts:

a, r	denote aileron and rudder servos, respectively
c	command signal
cg	center of gravity
t	vertical tail
wb	wing-body combination
e	error signal
ψ, ϕ, p	denote yaw, roll, and side-force information of feedback in autopilot loops, respectively

Dot over quantity indicates differentiation with respect to time.

Stability derivatives are indicated by subscript notation; for example,

$$C_{n\dot{\beta}} = \frac{\partial C_n}{\partial \dot{\beta}}$$

$$C_{n\dot{r}} = \frac{\partial C_n}{\partial \frac{rb}{2V}}$$

$$C_{l\dot{p}} = \frac{\partial C_l}{\partial \frac{pb}{2V}}$$

The stability system of axes is shown in figure 1.

DESCRIPTION OF AIRPLANE AND AUTOPILOTS

All calculations made in this paper are for a present-day fighter, jet-propelled airplane with unswept wings. A drawing of the airplane is shown in figure 2. This particular airplane is used in this study because frequency responses obtained from flight tests are available to check the calculated frequency responses. The derivatives and mass characteristics of the airplane are listed in table I. The stability derivatives are obtained from unpublished data.

The three types of autopilots which are studied in combination with the airplane can be described as follows:

(1) An autopilot designated the type 1 autopilot combines yaw damping (rudder moves in proportion to a yawing-velocity signal), heading stability (rudder moves in proportion to a heading error signal), and roll stability (ailerons move in proportion to a roll-angle error signal). This configuration was chosen for study because it represents, in an idealized form, a type of regulator autopilot that is being used at the present time.

(2) An autopilot designated the type 2 autopilot combines yaw damping, roll stability, a signal from the side force to the rudder (rudder moves in proportion to the side force to reduce the side force), and a signal from the heading to the ailerons (ailerons move in proportion to the heading error to correct the heading error by rolling the airplane). This configuration was chosen for study because it represents a type of fighter autopilot being used at the present time.

(3) An autopilot designated the type 3 autopilot combines yaw damping, heading stability, roll stability, and a signal from the side force to the ailerons (ailerons move in proportion to the side force to tilt the lift vector in the direction of the side force. This configuration was chosen for study because it has good response in both heading and course when a command is applied to the heading loop.

The autopilot loops which the different autopilots have in common are given the same gain in each case. These loops, the yaw-damping loop and the roll-stability loop, are given the gain recommended by the manufacturer of a type 2 autopilot for use with an airplane of the type studied in this investigation. Since there are no other autopilot loops placed inside the yaw-damping and the roll-stability loops in any of the autopilots studied that may change their optimum gain setting, it is reasonable to assume that they will have the same gain for each of the autopilots. The heading-stability-loop gain of the type 1 and type 3 autopilots is adjusted to give a closed-loop heading response to rudder deflection having a damping ratio of 0.3 (based on the assumption of a single degree of freedom in yaw with the yaw-damping gain mentioned previously).

One calculation with the type 2 autopilot is made with the gain relating the heading error signal to the aileron deflection and the gain relating the side-force signal to the rudder deflection set at the values recommended by the manufacturer of a type 2 autopilot. A second calculation is made in which the heading-error-signal gain is increased so that the steady-state roll angle resulting from a heading error for the type 2 autopilot will equal the steady-state roll angle resulting from a heading error for the type 3 autopilot. This gain adjustment affords a direct comparison between these two autopilots and, in addition, provides a rapid course response in each case. In the type 3 autopilot the gain between side force and aileron deflection is chosen to result in a roll angle of 1 radian for a side-force signal of 0.05g acceleration. All autopilot gains are listed in table II.

DESCRIPTION OF GUSTS

Two types of gusts are studied - side gusts, which add an increment to the angles of sideslip, and rolling gusts, which have the effect of adding an increment to the rolling velocity of the airplane with respect to the air mass. These gusts are assumed to vary sinusoidally. The use of sinusoidal disturbances appears to be appropriate for the study of the effects of turbulence, since flight data obtained in rough air show that the disturbances are of an irregular oscillatory nature and since such irregular disturbances can be reduced by generalized harmonic analysis to sinusoidal components of various frequencies and amplitudes. In this

paper the disturbances are restricted to side gusts and rolling gusts inasmuch as reference 2 has shown that the lateral effect of turbulence can be well approximated by gusts of these two forms. These gust forms are convenient to use since they are expressed by analytical terms that are similar to the terms for the variables β and $D\phi$ ordinarily used in equations of motion. Furthermore, references 2 and 3 show that the relative magnitude of the power spectral density of the side gusts diminishes as the square of the frequency and that the rolling gusts have a power spectral density that is constant throughout the frequency range considered in this paper.

The frequency range covered in this paper varies from 12 radians per second down to 0.2 radian per second. This range extends to well above the primary resonant frequency of the systems studied. The upper limit represents a gust wave length that is still large with respect to the length and span of the airplane. The lower limit of 0.2 radian per second was chosen because it was believed that information concerning gust frequency response is of little importance at lower frequencies inasmuch as the pilot or autopilot can easily control the low-frequency lateral motions. However, the lower limit is too high to show completely the effects of the spiral mode of the airplane with controls fixed.

METHOD OF ANALYSIS

Equations of Lateral Motion Including Gust Inputs

The equations of lateral motion used in this investigation are similar to those presented in reference 4. The usual procedure is varied by expressing separately the force and moment contributions of the wing-fuselage combination and the tail.

The equations written in nondimensional form are

$$\left. \begin{aligned}
 2\mu \left(\frac{DY}{V} + D\psi \right) &= C_{Y_{\beta_{wb}}} \beta_{cg} + C_{Y_{\beta_t}} \beta_t + \frac{1}{2} C_{Y_{P_{wb}}} D\phi_{cg} + \frac{1}{2} C_{Y_{P_t}} D\phi_t + \phi C_L + C_{Y_{\delta_r}} \delta_r + C_{Y_{\delta_a}} \delta_a \\
 2\mu \left(K_Z^2 D^2 \psi - K_{XZ} D^2 \phi \right) &= C_{n_{\beta_{wb}}} \beta_{cg} + \frac{1}{2} C_{n_{P_{wb}}} D\phi_{cg} + C_{n_{\beta_t}} \beta_t + \frac{1}{2} C_{n_{P_t}} D\phi_t + C_{n_{\delta_r}} \delta_r + C_{n_{\delta_a}} \delta_a \\
 2\mu \left(K_X^2 D^2 \phi - K_{XZ} D^2 \psi \right) &= C_{l_{\beta_{wb}}} \beta_{cg} + \frac{1}{2} C_{l_{P_{wb}}} D\phi_{cg} + \frac{1}{2} C_{l_{P_{wb}}} D\psi_{cg} + C_{l_{\beta_t}} \beta_t + \frac{1}{2} C_{l_{P_t}} D\phi_t + C_{l_{\delta_r}} \delta_r + C_{l_{\delta_a}} \delta_a
 \end{aligned} \right\} \quad (1)$$

In these equations the coefficients of the tail forces and moments ($C_{Y\beta_t}$, $C_{n\beta_t}$, etc.) are based on wing area and wing span.

In order to obtain the response to gusts from equations (1) the values of β_{cg} , β_t , ϕ_t , ϕ_{cg} , and ψ_{cg} must be expressed in terms of the gust inputs and the airplane motion. Derivation of the expression for these angles requires consideration of the assumed form of gust disturbance and the sidewash effects at the tail. The gust disturbance is divided into two separate modes - side gusts and rolling gusts. Side gusts are assumed to consist of lateral sinusoidal velocity variations within the air mass at right angles to the plane of symmetry of the airplane. Rolling gusts are assumed to consist of rotating sinusoidal velocity variations within the air mass and are assumed to rotate about the path of the airplane. At a given point in the air mass, the gust velocity is assumed not to change with time, and the wave length of the gust is assumed to be long compared with the length and span of the airplane.

The equations are solved for v/V , ψ , and ϕ in terms of the gust velocities. A side gust with velocity v_g will change the angle of sideslip of the airplane an amount equal to v_g/V ; that is, $\beta_g = v_g/V$. In addition, the airplane will have an angle of sideslip relative to still air equal to v/V ; $\beta_o = v/V$. Then the total angle of sideslip at the center of gravity is

$$\beta_{cg} = \beta_o + \beta_g$$

Likewise, the total rolling velocity of the airplane may be considered as consisting of the rolling velocity of the rolling gust and the rolling velocity of the airplane in still air:

$$D\phi_{cg} = D\phi + D\phi_g$$

Also,

$$\psi_{cg} = \psi$$

The angle of sideslip at the tail is assumed to be a function of the angle of sideslip of the airplane, the sideslip at the tail due to yawing velocity, and the sidewash angle resulting from wing lift which existed

when the wing was at a position now occupied by the tail. There is, therefore, a lag that occurs during the time required for a given lift disturbance at the wing to move back and cause some associated sidewash at the tail. This lag is proportional to the time required for the airplane to travel 1 tail length. Sidewash can be considered to arise from two sources: sidewash due to sideslip, both β_o and β_g ; and sidewash due to rolling velocity, both $D\phi$ and $D\phi_g$. Estimations of sidewash magnitude are given in references 5 and 6. The effect of β_g at the tail is assumed to lag behind the effect of β_g at the wing.

This lag describes the fact that a given gust disturbance is encountered at the center of gravity prior to being encountered at the tail. The expression for angle of sideslip of the tail expressed in nondimensional notation is

$$\begin{aligned} \beta_t = & \beta_o - l_x D\psi - \left(\beta_o \frac{\partial \sigma}{\partial \beta} \right)_{s=-l_x} - \left(D\phi \frac{\partial \sigma}{\partial D\phi} \right)_{s=-l_x} + \\ & \left(\beta_g \right)_{s=-l_x} - \left(\beta_g \frac{\partial \sigma}{\partial \beta} \right)_{s=-l_x} - \left(D\phi_g \frac{\partial \sigma}{\partial D\phi} \right)_{s=-l_x} \end{aligned} \quad (2)$$

The rolling velocity of the tail is assumed to equal the rolling velocity of the airplane and the rolling velocity of the gust, with lag to represent the effect mentioned previously:

$$D\phi_t = D\phi + \left(D\phi_g \right)_{s=-l_x} \quad (3)$$

The constant time lag $-l_x$ is expressed as $1 - l_x D$, which are the first two terms of a power-series expansion for a constant time lag. Using the expression $1 - l_x D$ to denote lag in sidewash has been shown to agree very well with experimental measurements of lag in sidewash.

Including these lag effects is an improvement over previous calculations which have neglected these effects. For a fighter airplane in the flight conditions used in this paper, the lag effects are negligible. The equations are set up in complete form for possible use where the effects may be more important. The lag in sidewash terms may be important for airplanes with sweptback wings or at flight conditions requiring high lift coefficients. The lag in gust effect at the tail is important for large airplanes, airplanes at low velocity, or airplanes with low-density ratios. These terms can be included with very little added complication.

The expression for angle of sideslip of the tail and the rolling velocity of the tail can now be written as follows:

$$\beta_t = \beta_o - l_x D\psi + \beta_g(1 - l_x D) - \beta_o \frac{\partial \sigma}{\partial \beta}(1 - l_x D) - \beta_g \frac{\partial \sigma}{\partial \beta}(1 - l_x D) - D\phi \frac{\partial \sigma}{\partial D\phi}(1 - l_x D) - D\phi_g \frac{\partial \sigma}{\partial D\phi}(1 - l_x D) \quad (4)$$

and

$$D\phi_t = D\phi + D\phi_g(1 - l_x D) \quad (5)$$

Substituting the expressions for β_{cg} , β_t , $D\phi_{cg}$, and $D\phi_t$ into the equations of motion (eqs. (1)) gives

$$\left. \begin{aligned} 2\mu D\beta_o + 2\mu D\dot{\gamma} - C_{Y\beta}\beta_o - \frac{1}{2}C_{YD\beta}D\beta_o - \frac{1}{2}C_{Yr}D\dot{\gamma} - \frac{1}{2}C_{Yp}D\phi - \frac{1}{2}C_{YD^2\phi}D^2\phi - \phi C_L - C_{Y\delta_r}\delta_r - C_{Y\delta_a}\delta_a = \\ C_{Y\beta}\beta_g + \frac{1}{2}(C_{YD\beta} + C_{Yr})D\beta_g + \frac{1}{2}C_{Yp}D\phi_g + \frac{1}{2}(C_{YD^2\phi} - C_{YD\phi_t})D^2\phi_g \\ 2\mu K_Z^2 D^2\dot{\psi} - 2\mu K_{ZZ}D^2\phi - C_{n\beta}\beta_o - \frac{1}{2}C_{nD\beta}D\beta_o - \frac{1}{2}C_{nr}D\dot{\gamma} - \frac{1}{2}C_{np}D\phi - \frac{1}{2}C_{nD^2\phi}D^2\phi - C_{n\delta_r}\delta_r - C_{n\delta_a}\delta_a = \\ C_{n\beta}\beta_g + \frac{1}{2}(C_{nD\beta} + C_{nr})D\beta_g + \frac{1}{2}C_{np}D\phi_g + \frac{1}{2}(C_{nD^2\phi} - C_{nD\phi_t})D^2\phi_g \\ 2\mu K_X^2 D^2\phi - 2\mu K_{XX}D^2\dot{\psi} - C_{l\beta}\beta_o - \frac{1}{2}C_{lD\beta}D\beta_o - \frac{1}{2}C_{lr}D\dot{\gamma} - \frac{1}{2}C_{lp}D\phi - \frac{1}{2}C_{lD^2\phi}D^2\phi - C_{l\delta_r}\delta_r - C_{l\delta_a}\delta_a = \\ C_{l\beta}\beta_g + \frac{1}{2}(C_{lD\beta} + C_{lr})D\beta_g + \frac{1}{2}C_{lp}D\phi_g + \frac{1}{2}(C_{lD^2\phi} - C_{lD\phi_t})D^2\phi_g \end{aligned} \right\} \quad (6)$$

where

$$\begin{aligned}
 C_{Y_{\beta}} &= C_{Y_{\beta_{wb}}} + C_{Y_{\beta_t}} \left(1 - \frac{\partial \sigma}{\partial \beta}\right) & C_{n_{\beta}} &= C_{n_{\beta_{wb}}} + C_{n_{\beta_t}} \left(1 - \frac{\partial \sigma}{\partial \beta}\right) & C_{l_{\beta}} &= C_{l_{\beta_{wb}}} + C_{l_{\beta_t}} \left(1 - \frac{\partial \sigma}{\partial \beta}\right) \\
 C_{Y_{D\beta}} &= 2l_x \frac{\partial \sigma}{\partial \beta} C_{Y_{\beta_t}} & C_{n_{D\beta}} &= 2l_x \frac{\partial \sigma}{\partial \beta} C_{n_{\beta_t}} & C_{l_{D\beta}} &= 2l_x \frac{\partial \sigma}{\partial \beta} C_{l_{\beta_t}} \\
 C_{Y_r} &= -2l_x C_{Y_{\beta_t}} & C_{n_r} &= -2l_x C_{n_{\beta_t}} & C_{l_r} &= C_{l_{r_{wb}}} - 2l_x C_{l_{\beta_t}} \\
 C_{Y_p} &= C_{Y_{p_{wb}}} + C_{Y_{\beta_t}} 2 \left(l_z - \frac{\partial \sigma}{\partial D\phi}\right) & C_{n_p} &= C_{n_{p_{wb}}} + C_{n_{\beta_t}} 2 \left(l_z - \frac{\partial \sigma}{\partial D\phi}\right) & C_{l_p} &= C_{l_{p_{wb}}} + C_{l_{\beta_t}} 2 \left(l_z - \frac{\partial \sigma}{\partial D\phi}\right) \\
 C_{Y_{D^2\phi}} &= 2l_x \frac{\partial \sigma}{\partial D\phi} C_{Y_{\beta_t}} & C_{n_{D^2\phi}} &= 2l_x \frac{\partial \sigma}{\partial D\phi} C_{n_{\beta_t}} & C_{l_{D^2\phi}} &= 2l_x \frac{\partial \sigma}{\partial D\phi} C_{l_{\beta_t}} \\
 C_{Y_{Dp_t}} &= 2l_x l_z C_{Y_{\beta_t}} & C_{n_{Dp_t}} &= 2l_x l_z C_{n_{\beta_t}} & C_{l_{Dp_t}} &= 2l_x l_z C_{l_{\beta_t}} \\
 & & & & C_{l_{r_t}} &= -2l_x C_{l_{\beta_t}}
 \end{aligned}$$

Note that

$$\begin{aligned}
 C_{Y_{p_t}} &= 2l_z C_{Y_{\beta_t}} & C_{n_{p_t}} &= 2l_z C_{n_{\beta_t}} & C_{l_{p_t}} &= 2l_z C_{l_{\beta_t}}
 \end{aligned}$$

The terms involving $D\beta_g$ and $D^2\phi_g$ on the right-hand side of equations (6) result from the lag in sidewash and from the lag between the effects of a gust on the wing and on the tail as the airplane passes a given point in the air mass.

Calculation of Response to Sinusoidal Gust Disturbances

Airplane with controls fixed.- To determine the steady-state response of the airplane to a sinusoidal gust disturbance when the controls are fixed, terms involving δ_r and δ_a are set equal to zero. The equations of motion can then be solved simultaneously (for example, by the method of determinants) to obtain the variables β_0 , ψ , and ϕ in terms of β_g and $D\phi_g$. The steady-state response to a sinusoidal input can then be found by substituting $D = i\omega$ into the resulting expressions, which are known as the transfer functions.

Airplane-autopilot combinations.- A second aspect of the airplane gust response studied was the motions of the airplane encountered when autopilot loops were incorporated in the airplane to regulate some of the variables. Of the many methods of analysis available for determining the response of an airplane-autopilot combination, two methods were used: an approach using the equations of motion and an approach using component transfer functions. For each calculation the autopilot servomechanisms were assumed to have perfect response (no lag and constant amplitude) over the range of frequencies of interest in the calculations of the airplane response. Therefore, the transfer functions of the autopilot servo were expressed as gains.

In the equation-of-motion method of calculation, the effects of the autopilot loops were included as equivalent stability derivatives. This substitution was possible because the assumption of a perfect servo makes the forces and moments applied by the autopilot on the airplane explicit functions of the motion of the airplane. A three-degree-of-freedom response for the airplane including these artificial stability derivatives was obtained. The analysis was not significantly more complicated than that required to obtain the response of the airplane with controls fixed. The calculation was repeated for the airplane in combination with each of the three autopilots described previously. The equivalent stability derivatives are listed in table II beside the autopilot gains from which they were derived.

The transfer-function method of analysis also was used in this investigation to present examples of the application of this type of calculation in the determination of the response to gusts. This method is very useful to engineers in establishing optimum autopilot gains, since it affords a direct study of the effects of gain change on the system. The method is also used for cases in which the operation of the autopilot cannot be expressed analytically. Many times in such cases the actual autopilot equipment is used in conjunction with the analog-computing equipment.

The transfer-function method is carried out by combining the transfer functions of the airplane with the transfer functions of the autopilot in a manner that is discussed in reference 7. A block diagram illustrating this method is shown in figure 3. In general, the transfer function of an actual autopilot servo would be frequency-variant and would be expressed by a function of second order, or higher. However, as was stated before, the autopilot servos are assumed to be perfect since study of the effect of variations of servo performance was considered beyond the scope of the present investigation.

Even with this simplified assumption for the autopilot servos, the combination of a three-degree-of-freedom airplane with an autopilot according to the scheme shown in figure 3 will result in a system transfer function having polynomials of approximately the fourteenth order. If servo dynamics were included, the order of the transfer function would be even higher.

Since it is very difficult to study parameter change with transfer functions of this complexity, various simplifications were tried in an attempt to find the simplest form of system transfer function that would give an answer consistent with the results obtained from the analysis of the equations of motion previously discussed. Details of these simplifications are given in the appendix.

A comparison of the equation-of-motion method of analysis with the transfer-function method is interesting. The equation-of-motion method using the artificial stability derivatives and the transfer-function method describing a three-degree-of-freedom airplane and using the simplified assumptions for the autopilot servos both express the same system; the only difference is that the equation-of-motion method results in a system transfer function of the fifth order and the transfer-function method results in a system transfer function of the fourteenth order. These facts lead to the conclusion that there are factors in the numerator and denominator of the system transfer function obtained by the transfer-function method that could be extracted so as to reduce the order. However, extraction of these factors is too difficult to be useful in simplifying the method.

Calculation of Power Spectral Density of Airplane Motion

The power spectral density of the side gusts β_g and the rolling gust $D\phi_g$ were derived from reference 2 and are plotted in figure 4. The square of the frequency response to β_g and $D\phi_g$ of the motion of the airplane as obtained by the equation-of-motion method was multiplied by the corresponding power spectral density of the gust to determine the power spectral density of the motion of the airplane. These curves have

been stopped at the low-frequency limit at which the variation of the power spectral density for the side gusts appears to break. Recent information indicates that this falling off occurs at gust wave lengths of approximately 6,000 feet.

Calculation of Frequency Response to Command Inputs

General.- As a point of additional interest, the heading response to a heading command and the course response to a heading command for the airplane-autopilot combinations are also calculated. The command response considered in this paper is one that results from applying the command to the particular autopilot channel that is used to regulate the variable being commanded. In the case of pilot-applied heading or course commands for the type 1 autopilot, this method is not usually used because such commands are applied to the aileron loop while the heading regulation supplied by the yaw loop is rendered inoperative during the command operation. When commands result from tying the airplane to an external reference, such as radar tracking of a target or beam following, it is not possible to utilize separate loops for command and regulation. Systems in which the same loop is used for command and regulation are considered herein.

Type 1 autopilot.- The heading response under the foregoing conditions for the type 1 autopilot may be determined as the response to a rudder deflection, and the course response may be determined as the response of the path of the airplane to a rudder deflection. The heading response ψ/ψ_c is determined by using a rudder input in the equations of motion, similar to the procedure used to determine heading response to side gusts ψ/β_g . The expression for the course response to a heading command is developed as follows:

$$\kappa = \psi + \beta_o$$

$$\frac{\kappa}{\psi_c} = \frac{\psi}{\psi_c} + \frac{\beta_o}{\psi_c}$$

$$= \frac{\psi}{\psi_c} + \frac{\beta_o}{\psi} \frac{\psi}{\psi_c}$$

$$= \frac{\psi}{\psi_c} \left(1 + \frac{\beta_o}{\psi} \right)$$

where β_0/ψ is the ratio of the quantities β_0/δ_r and ψ/δ_r , which were obtained from the equations of motion.

Type 2 autopilot.— In determining the response to a heading command for the type 2 autopilot, the heading signals go to the aileron loop. With the lateral force held to small values by the side-force component of the autopilot, the resulting heading and course changes are the same. These responses are obtained by assuming that the horizontal sideways force, horizontal acceleration, and consequently the rate of change of heading and course are proportional to the roll angle ϕ . The horizontal sideways acceleration is integrated to obtain the change in heading or course. The development of the equations of these relationships is as follows. The open-loop response of ϕ to the error signal is

$$\frac{\phi}{\psi_e} = \frac{K_\psi \frac{\phi}{\delta_a} K_a}{1 + K_\phi \frac{\phi}{\delta_a} K_a}$$

The relationship between ψ and ϕ is

$$\psi = \frac{\phi g b}{v^2_D}$$

Therefore, the closed-loop response to a heading command is

$$\frac{\psi}{\psi_c} = \frac{\kappa}{\psi_c} = \frac{\frac{K_\psi \frac{\phi}{\delta_a} K_a}{1 + K_\phi \frac{\phi}{\delta_a} K_a} \frac{g b}{v^2_D}}{1 + \frac{K_\psi \frac{\phi}{\delta_a} K_a}{1 + K_\phi \frac{\phi}{\delta_a} K_a} \frac{g b}{v^2_D}} \quad (7)$$

Type 3 autopilot.— The heading response ψ/ψ_c for the airplane in combination with the type 3 autopilot is obtained in the same manner as for the type 1 autopilot. In order to determine the course response to a heading command, the open-loop response of ϕ to the error signal ψ_e is obtained by including a signal in the roll equation that results from the coupling of side force to aileron deflection of the autopilot. This signal, which is similar to an equivalent stability derivative, is given in table II. The resulting value of ϕ/ψ_e is treated in the same way as for the type 2 autopilot case. The horizontal sideways acceleration was assumed to be proportional to ϕ , and this acceleration was integrated to give the change in course. This open-loop response was closed with a unity feedback to give values of κ/ψ_c .

RESULTS

Frequency Response of Airplane With Controls Fixed

The response to side gusts and to rolling gusts of the airplane with controls fixed is shown in figure 5. These results show that, at low frequencies, the yaw response to side gusts ψ/β_g is approaching a value of 1.0; this trend indicates that the airplane yaws into the gust. The same result can be stated another way by saying that β is approaching zero at low frequencies. The roll response to side gusts ϕ/β_g is primarily the result of the $C_{l\beta}$ coupling. A large resonance occurs at the frequency of the Dutch roll oscillation of the airplane. The same resonance appears in the response to rolling gusts. These resonance peaks are due to the low damping of the Dutch roll mode, a characteristic that is fairly typical of present-day fighter airplanes. Moreover, the roll response to side gusts is larger than the roll response to rolling gusts at the peak frequency whereas the comparison is reversed at higher and lower frequencies because the Dutch roll mode is excited more by side gusts than by rolling gusts.

Frequency Response of Airplane-Autopilot Combinations

Type 1 autopilot.— The frequency response of the airplane in combination with the type 1 autopilot is shown in figure 6. When the airplane was combined with the type 1 autopilot, the resonant peaks that were present in the responses of the airplane with controls fixed were greatly reduced, and the amplitude ratio of the ψ/β_g responses was reduced by a factor of approximately 10 in the low frequency range. The additional heading stability provided by the autopilot approximately doubled the peak frequency of the ψ/β_g response over that of the airplane with controls

fixed. Since the airplane was restrained from heading into the gust, β was increased beyond the values for the condition of fixed controls, and, in spite of the fact that the autopilot stabilized the airplane in roll, an increase in the ϕ/β_g response resulted at low frequencies. The roll response could be reduced by increasing the roll loop gain. The roll gain used in this calculation is relatively small, and, with some types of autopilot servos in present-day use, a higher gain could be used without encountering objectionable characteristics. The roll stability added by the autopilot produced a new resonant peak for the roll response at a frequency which is not very different from that of the peak of the airplane with controls fixed due to the Dutch roll oscillation. The roll response to rolling gusts $\phi/D\phi_g$ was greatly reduced at low frequencies by the autopilot.

The results of calculations of a simplified block diagram also are plotted in figure 6 for comparison with the results of the three-degree-of-freedom equation of motion. The amplitude ratio and the phase angle of the yaw response to rolling gusts $\psi/D\phi_g$ at low frequencies for the simplified calculation do not agree with those for the three-degree-of-freedom calculation. The predicted amplitude in both cases is small, and this fact is probably the reason for the poor agreement. Although in some applications of frequency-response techniques - for example, in the study of the open-loop response of a mechanism - such a phase-angle error would be unacceptable, the phase relationships are not believed to be particularly significant when gust inputs are considered.

In addition, the control-deflection frequency response as calculated by the transfer-function method is also plotted in figure 6. The figure shows that there are only small variations in amplitude ratio and phase angle with frequency up to the peak frequency. At higher frequencies the inertia effects attenuate the airplane response, and consequently the control deflections are reduced also.

Type 2 autopilot. - When the airplane is combined with the type 2 autopilot with the lower value ($K_\psi = 23$ volts/radian) for the autopilot coupling between ψ and δ_a , the response to a side gust, as shown in figure 7, indicates that the resonant peaks have been greatly reduced. The low-frequency values of ψ/β_g are the same as for the airplane with controls fixed; the similarity is to be expected since the side-force component of the autopilot aids the airplane in turning into the gust. The values of ϕ/β_g are increased at the low frequencies by the autopilot coupling between ψ and ϕ . The plot of the response to rolling gusts (fig. 7(b)) shows that the incorporation of roll stability has reduced the $\phi/D\phi_g$ response at low frequencies. The $\psi/D\phi_g$ response is small, although it is somewhat greater than that obtained with the type 1 autopilot, particularly at low frequencies. Once again the

results of the simplified block-diagram method are plotted with the results of the three-degree-of-freedom equation of motion for comparison. It can be seen that some discrepancies occur in the two calculations for $\psi/D\phi_g$. The control-deflection curves show a rapid increase in rudder amplitude ratio with increase in gust frequency. The aileron amplitude ratio for side gusts follows the variation of ψ/β_g and has the same phase angle. Both the variations of $\phi/D\phi_g$ and $\delta_a/D\phi_g$ as calculated by the simplified method are exactly the same as for the type 1 autopilot.

When the autopilot coupling between ψ and δ_a is increased ($K_\psi = 114$ volts/radian), the ϕ/β_g response is also increased. (See fig. 8.) This coupling, discussed subsequently, was increased to provide better heading response to a heading command, and this heading-response improvement is obtained at the expense of a higher amplitude ratio for ϕ/β_g . The effect of the large roll angles that occur at low frequencies with the type 2 autopilot causes a reduction in the ψ/β_g response. The simplified block-diagram method of calculating ψ/β_g , $\phi/D\phi_g$, and $\psi/D\phi_g$ is the same as for the case with $K_\psi = 23$ volts/radian. The effect of the large roll response to side gusts, which was ignored in the simplified calculations, results in discrepancies between the simplified solutions and the equation-of-motion solutions at low frequencies.

Type 3 autopilot.— The results of the airplane in combination with the type 3 autopilot are shown in figure 9. The coupling between side force and aileron deflection, which was included to provide good course response to a heading command, caused a large roll response to side gusts to occur. The ψ/β_g response is the same as for the airplane in combination with the type 1 autopilot with the exception that the large roll angle that occurs at low frequencies with this configuration causes a reduction in the ψ/β_g response. The response to rolling gusts is, in general, of the same order of magnitude as for the other combinations.

The simplified block-diagram solutions for the airplane in combination with the type 3 autopilot are in poor agreement with the equation-of-motion solutions. The simplified solution for ψ/β_g is in error because it did not account for the effects of the large roll angles that occur. The solution for ϕ/β_g is in error because the simplified expression for ψ/β_g is included in the expression for ϕ/β_g ; and, because of the large coupling between side force and roll angle, the solution of ϕ/β_g is very sensitive to any errors in ψ/β_g . Thus, even the minor errors in the simplified ψ/β_g response at high frequencies are reflected as large errors in the ϕ/β_g response. A modified solution for ϕ/β_g , in which a three-degree-of-freedom ψ/β_g response, where the yaw loops of the autopilot were included as equivalent stability derivatives, did show

good agreement with the equation-of-motion solution. (See fig. 9.) The modified solution also demonstrated the reason for the unusual shape of the frequency-response curve for ϕ/β_g . The increase in ϕ/β_g with frequency at low frequencies is caused by the increase in side force due to sideslip and the coupling between side force and roll angle. Above a frequency of 0.1 radian/span, the side force due to rudder deflection increases rapidly and with an opposite sign from the side force due to sideslip, until at $\omega = 0.22$ radian/span the two effects approximately cancel. At frequencies higher than $\omega = 0.22$ radian/span, the side force due to rudder deflection and the side force due to sideslip become in phase; the result is an increase in side force and consequently in ϕ/β_g . This increase continues until the inertia effects attenuate the response.

The simplified solutions for $\psi/D\phi_g$ and $\phi/D\phi_g$ are identical to the solution for the type 1 autopilot, but are in only fair agreement with the equation-of-motion solutions. A modified solution for $\phi/D\phi_g$ similar to that described for ϕ/β_g , also shown in figure 9, gave a response that was in good agreement with the equation-of-motion solution.

Power Spectral Density of Airplane Motion

The power spectral density of the motion of the airplane in response to gusts is shown in figure 10. These plots emphasize the greater relative importance of the low-frequency side-gust components over the high-frequency components and the greater relative importance of the side gust over the entire frequency range compared with the rolling gusts in producing motions of the airplane. The area under these curves over any particular frequency is proportional to the mean square of the part of the airplane motion contributed by those frequencies. Aside from these general conclusions, the power-spectral-density plots also show the variations between configurations that were noted previously in the discussion on the frequency response. These similarities existed in the cases considered in this paper inasmuch as all comparisons were made for restricted frequency ranges.

Summary of Results on the Response to Gusts

When the airplane was combined with the various autopilots, in all cases the Dutch roll resonance was greatly reduced. The heading stability provided by the type 1 autopilot maintained good regulation in yaw, but the increase in sideslip at low frequencies resulted in a moderate increase in roll response to side gusts. This roll response could have been reduced if greater roll stability had been provided by the autopilot. The response to rolling gusts was well regulated. When the airplane was combined with the type 2 autopilot, the airplane yawed into the gust to

reduce sideslip, and the coupling between heading error and aileron deflection caused large roll response to side gusts. The response to rolling gusts was approximately the same as for the type 1 autopilot. When the airplane was combined with the type 3 autopilot, good regulation in yaw was maintained. The coupling between side force and aileron deflection caused large roll response to side gusts. The response to rolling gusts was well regulated.

Response to Heading Commands for the Airplane-Autopilot Combinations

In order to complete more nearly the information necessary for evaluation of the different autopilots discussed in this paper, the response to heading commands for each of the airplane-autopilot combinations is also given. The heading response to a heading command for all cases is plotted in figure 11, and the course response is plotted in figure 12.

The excellent heading response to a heading command for the airplane in combination with the type 1 and type 3 autopilots is illustrated in figure 11. Each maintains an amplitude ratio of approximately 1 out to frequencies well beyond the Dutch roll frequency of the basic airplane. The heading response of the airplane with the type 2 autopilot is the poorest. However, increasing the coupling of ψ to ϕ improves the heading response. The larger value of the coupling of ψ to ϕ used in the calculations was chosen to give the same static ratio of roll angle to heading command as the type 3 autopilot. Therefore, the frequency response for these two cases can be compared directly.

A comparison of the course response to heading commands for the three autopilots (fig. 12) indicates faster course response for the type 2 and type 3 autopilots than for the type 1 autopilot. The reason for this difference is that for the type 1 autopilot only side force is available for producing horizontal-path changes, since, as was explained before, in the present study the command was restricted to the yaw loop. For the type 2 and type 3 autopilots the lift force is tilted to provide a horizontal component of acceleration. The type 3 autopilot combines both the good heading response of the type 1 autopilot, by including the same heading-stability loop as the type 1 autopilot, and an excellent course response, by adding the coupling between side force and roll angle which tilts the lift vector.

In many flight operations, it is desirable to have rapid course response to automatic lateral commands, such as for rocket-armed fighter operations or for beam riding. It is also desirable to regulate sideslip during pilot-commanded lateral maneuvers. However, the methods incorporated to provide good course response and to regulate sideslip in the autopilot configurations considered in this paper result in large roll

response to side gusts. It might be possible to provide a dual mode of operation that would provide sideslip regulation at low frequencies and heading regulation at high frequencies. Since $\psi = \beta_0$ at high frequencies, this arrangement would provide sideslip regulation throughout the frequency range insofar as command maneuvers are concerned and would avoid the large roll motions that occur because of high-frequency side gusts.

CONCLUDING REMARKS

In developing the equations of motion as used in this paper to express motion due to gusts, terms involving sidewash at the tail and expressing lag effect of the gust at the tail were used. However, for the airplane configuration used in these calculations, these terms had little or no effect and could have been neglected. For airplanes with sweptback wings or for high values of lift coefficient, these terms may become significant. The lag term which represents the lag in gust effect at the tail may be important for large airplanes, airplanes flying at low speed, or airplanes with low-density ratios.

The response of the airplane with controls fixed exhibited a large resonance associated with the Dutch roll mode. This resonance response was particularly noticeable in the roll response to side gusts. This feature of a poorly damped Dutch roll mode that is excited by side gust is typical of present-day fighter airplanes. At low frequencies the airplane yawed into the gusts and reduced sideslip due to gusts.

For cases in which various attitude autopilots were combined with the airplane, the following changes to the response of the airplane with controls fixed are noted:

(1) When the airplane was combined with an autopilot that supplied yaw damping, heading stability, and roll stability, the increase in sideslip at low frequencies resulted in a moderate increase in roll response to side gusts. The heading stability maintained good regulation in yaw.

(2) When the autopilot supplied yaw damping, roll stability, a coupling between the heading error and the aileron deflection, and a coupling between side force and rudder deflection, the airplane yawed into the gust in order to regulate side force and, consequently, sideslip. The coupling between heading error and roll angle caused large roll response to side gusts.

(3) When the autopilot supplied yaw damping, heading stability, roll stability, and a coupling between side force and aileron deflection, the heading stability again maintained good regulation in yaw. The coupling between side force and aileron deflection caused a large roll response to side gusts.

(4) In all three cases the yaw damping eliminated the resonant Dutch roll response to gusts. Also, in all three cases the roll response to rolling gusts was approximately the same, with the roll stability added by the autopilot maintaining good regulation in roll.

In the last two cases, the type 2 autopilot with a heading-stability gain of 114 volts/radian and the type 3 autopilot, the features that produced good course response to heading commands caused large roll response to side gusts to occur; this response was in contrast to the better roll response of the airplane in combination with the type 1 autopilot.

The simplified method of calculation predicted the important motions of the airplane with good accuracy. Some discrepancies were noted in the predicted amplitude of the small motions. However, since the trends of the changes in the motion of the airplane with changes in autopilot configuration were accurately predicted and since the peak frequencies were accurately predicted, it appears that the simplified method could be used for gust studies.

Langley Aeronautical Laboratory,
National Advisory Committee for Aeronautics,
Langley Field, Va., October 28, 1955.

APPENDIX

CALCULATION OF FREQUENCY RESPONSE OF AIRPLANE-AUTOPILOT

COMBINATIONS BY TRANSFER-FUNCTION METHOD

The details of the simplifications and the steps in calculating the frequency response of the airplane-autopilot combinations by the transfer-function method of analysis are described. The simplifications that were examined generally consisted in attempting to decrease the number of terms in equations (6) by reducing the degrees of freedom involved in the calculations. Motions other than the particular one being studied were ignored either because they were small or because they were controlled by some component of the autopilot and, therefore, did not influence the motion of the airplane in the mode being studied. The assumption that a particular motion can be ignored because it is controlled by some component of the autopilot is subject to the performance of that component. The loop gain must be large enough to regulate the variable to a point where it can be ignored, and the dynamics of the loop must be good enough to provide this regulation throughout the frequency range being studied.

Type 1 Autopilot

For the airplane in combination with the type 1 autopilot, the responses in ψ , ϕ , δ_r , and δ_a to side gusts and rolling gusts were calculated. A block diagram of the autopilot setup is shown in figure 13. Since the airplane was controlled in roll, freedom in roll is ignored when calculating ψ/β_g . Also, since the side force of the airplane was small in comparison with the yawing moments on the airplane, freedom in lateral displacement is ignored, and ψ is assumed to equal $-\beta_0$. On this basis, ψ/β_g and ψ/δ_r for the airplane with no autopilot yaw components are obtained by considering an airplane with a single degree of freedom in yaw. This airplane was combined with the autopilot components as shown in figure 13 to obtain the response of the controlled airplane.

In order to obtain ϕ/β_g for the controlled airplane, the strong coupling between ϕ and β due to dihedral effect must be considered. In this case, since ψ is controlled, freedoms in yaw and lateral displacement are ignored, and both ψ and β_0 are assumed to be equal to zero. Then, from the simplified roll equation (obtained from eqs. (6)) an expression for ϕ/β of the airplane with controls fixed is determined. If β is assumed equal to β_g , the quantity ϕ/β_g for the airplane

without roll control can be determined. This response of the airplane to β_g is added to the single-degree-of-freedom response of the airplane to δ_a in a manner indicated by the block diagram of figure 13 to give the controlled-airplane response to β_g . The assumption that $\beta = \beta_g$ will be increasingly in error as the frequency is reduced because the airplane will drift with the gust at very low frequencies. However, at $\omega = 0.01$ radians/span this assumption is still accurate enough for practical purposes.

In the determination of the roll response to rolling gusts $\phi/D\phi_g$, the freedoms in yaw and lateral displacement are ignored for the reasons given previously, and the response is obtained by considering an airplane with a single degree of freedom in roll in combination with the autopilot loops as shown in figure 13(b).

In order to obtain the yaw response ψ to rolling gusts $D\phi_g$, the couplings between ϕ and ψ , ϕ and β , and β and ψ must be considered. Therefore, an expression for ψ/ϕ containing these couplings is determined from the simplified yaw and side-force equations (obtained from eqs. (6)). This expression is used to relate the homogeneous response of ψ to ϕ . This response in ψ is added to a single-degree-of-freedom yaw response to rudder deflection, in which the rudder deflection is controlled by the yaw components of the autopilot, as is shown in figure 13. The $\psi/D\phi_g$ response is then obtained by multiplying the ψ/ϕ response of the controlled airplane by the previously determined $\phi/D\phi_g$ response.

Type 2 Autopilot

The various responses of the airplane in combination with the type 2 autopilot are calculated in the same basic manner as for the type 1 autopilot combination except for the following changes in detail. Since the side force of the airplane is small and since the airplane is stabilized in roll by the autopilot, the roll and lateral displacements are ignored in representing the airplane in yaw with controls fixed. Again ψ is assumed to equal $-\beta_0$. In order to establish the effect of the autopilot side-force loop, the side force, even though it is small, must be calculated. From the equations of motion it can be seen that the nondimensional side force is

$$C_Y = C_{Y_\beta} \beta + C_{Y_{\delta_r}} \delta_r$$

An expression for β in terms of the controlled-airplane response and β_g is

$$\begin{aligned}\beta &= \beta_o + \beta_g \\ &= -\frac{\psi}{\beta_g}\beta_g + \beta_g\end{aligned}\quad (A1)$$

The block diagram of figure 14(a) illustrates how the side-force and yawing-velocity feedbacks are included in determining ψ/β_g of the controlled airplane.

The variable ψ is used as an input to the aileron servo in the type 2 autopilot. Therefore, an expression containing this autopilot coupling and the aerodynamic coupling between ϕ and β is necessary to determine the ϕ/β_g response. The aerodynamic coupling is included as was done for the calculation of the type 1 autopilot, with β determined by the equation (A1). Figure 14 illustrates the manner of combining the transfer functions to determine the ϕ/β_g response.

In the determination of the roll response to rolling gusts $\phi/D\phi_g$, the autopilot coupling between ψ and ϕ should be included as was done before in determining ϕ/β_g . However, because of the very small aerodynamic coupling between ϕ and ψ , it was believed that the $\psi/D\phi_g$ response would be very small and that the yaw signal to the ailerons could be neglected. The response of ϕ to $D\phi_g$ is obtained from a single-degree-of-freedom calculation illustrated by the block diagram of figure 14(b). With a value for $\phi/D\phi_g$ determined, it is possible to obtain $\psi/D\phi_g$ in a manner similar to that used for the type 1 autopilot.

Type 3 Autopilot

For the airplane in combination with the type 3 autopilot, the block-diagram method of calculation for ψ/β_g is identical with that for the airplane in combination with the type 1 autopilot. Since the autopilot coupling between side force and aileron deflection is very strong in this case, it is recognized that the resulting large angle of roll ϕ might influence the motion in yaw response ψ at low frequencies. No method for including the roll effect could be devised; and, as a result, it is to be expected that these calculations will show more error in the lower range of frequencies than the block-diagram calculations used in the other cases.

In order to determine ϕ/β_g , side force is determined as was done in the calculations for the type 2 autopilot, and this side force is used as an input to the aileron servo. The response of ϕ of the uncontrolled airplane is determined from a consideration of a single degree of freedom in roll as was done in the case of the type 1 autopilot. The sum of the airplane response of ϕ to β_g and the airplane response to the aileron deflection which resulted from the side-force input and the roll-stabilization feedback of the autopilot gives the controlled-airplane response. In determining the side force, β is assumed to be composed of $-\psi$, β_g , and the increment of β resulting from the lateral velocity of the airplane that arises because of the roll angle. The block diagram representing the analysis is shown in figure 15(a).

The simplified block-diagram method of calculating the responses to rolling gusts (fig. 15(b)) is the same as for the airplane in combination with the type 1 autopilot.

REFERENCES

1. Phillips, William H., and Kraft, Christopher C., Jr.: Theoretical Study of Some Methods for Increasing the Smoothness of Flight Through Rough Air. NACA TN 2416, 1951.
2. Summers, Robert A.: A Statistical Description of Large-Scale Atmospheric Turbulence. Sc. D. Thesis, M.I.T., 1954. (Also Rep. T-55, Instrumentation Lab., M.I.T., May 17, 1954.)
3. Decaulne, Paul: Airplane Lateral Response to Statistical Gust Inputs. M. S. Thesis, M.I.T., 1952.
4. Sternfield, Leonard: Effect of Automatic Stabilization on the Lateral Oscillatory Stability of a Hypothetical Airplane at Supersonic Speeds. NACA TN 1818, 1949.
5. Michael, William H., Jr.: Analysis of the Effects of Wing Interference on the Tail Contributions to the Rolling Derivatives. NACA Rep. 1086, 1952. (Supersedes NACA TN 2332.)
6. Goodman, Alex: Effects of Wing Position and Horizontal-Tail Position on the Static Stability Characteristics of Models With Unswept and 45° Sweptback Surfaces With Some Reference to Mutual Interference. NACA TN 2504, 1951.
7. Gardner, Murray F., and Barnes, John L.: Transients in Linear Systems Studied by the Laplace Transformation. Lumped-Constant Systems. Vol. I, John Wiley & Sons, Inc., 1942.

TABLE I.- CHARACTERISTICS OF AIRPLANE USED IN CALCULATIONS

Physical characteristics:

Weight, lb	12,600
Radius of gyration about X-axis k_X , ft	4.30
Radius of gyration about Z-axis k_Z , ft	7.91
Wing area, sq ft	250
Vertical tail area, sq ft	55
Wing span, ft	35.25
Tail length, ft	15
Distance from thrust line to center of area of vertical tail, ft	5.32

Flight conditions:

Airspeed, ft/sec	695
Altitude, ft	30,000
Mach number	0.7

Nondimensional data:

μ	50
l_x	0.42
l_z	0.112
K_X^2	0.01485
K_Z^2	0.0504
K_{XZ}	0.00062
C_L	0.242

Aerodynamic parameters:

Side force		Yawing		Rolling	
$C_{Y_{\beta_{wb}}}$	-0.05	$C_{n_{\beta_{wb}}}$	-0.055	$C_{l_{\beta_{wb}}}$	-0.11
$C_{Y_{\beta_t}}$	-0.53	$C_{n_{\beta_t}}$	0.175	$C_{l_{\beta_t}}$	-0.05
$C_{Y_{D\beta}}$	0	$C_{n_{D\beta}}$	0	$C_{l_{D\beta}}$	0
$C_{Y_{p_{wb}}}$	0	$C_{n_{p_{wb}}}$	-0.039	$C_{l_{p_{wb}}}$	-0.45
$C_{Y_{D^2\phi}}$	-0.045	$C_{n_{D^2\phi}}$	0.0147	$C_{l_{D^2\phi}}$	-0.005
$C_{Y_{Dp_t}}$	-0.050	$C_{n_{Dp_t}}$	0.0204	$C_{l_{Dp_t}}$	-0.005
$C_{Y_{\delta_r}}$	0.228	$C_{n_{\delta_r}}$	-0.077	$C_{l_{\delta_r}}$	0.026
$C_{Y_{\delta_a}}$	0	$C_{n_{\delta_a}}$	0	$C_{l_{\delta_a}}$	-0.086
C_{Y_r}	0.45	C_{n_r}	-0.147	$C_{l_{r_{wb}}}$	0.004
				$C_{l_{rt}}$	0.050

Sidewash

$\frac{\partial \sigma}{\partial \beta}$	0
$\frac{\partial \sigma}{\partial D\phi}$	0.10

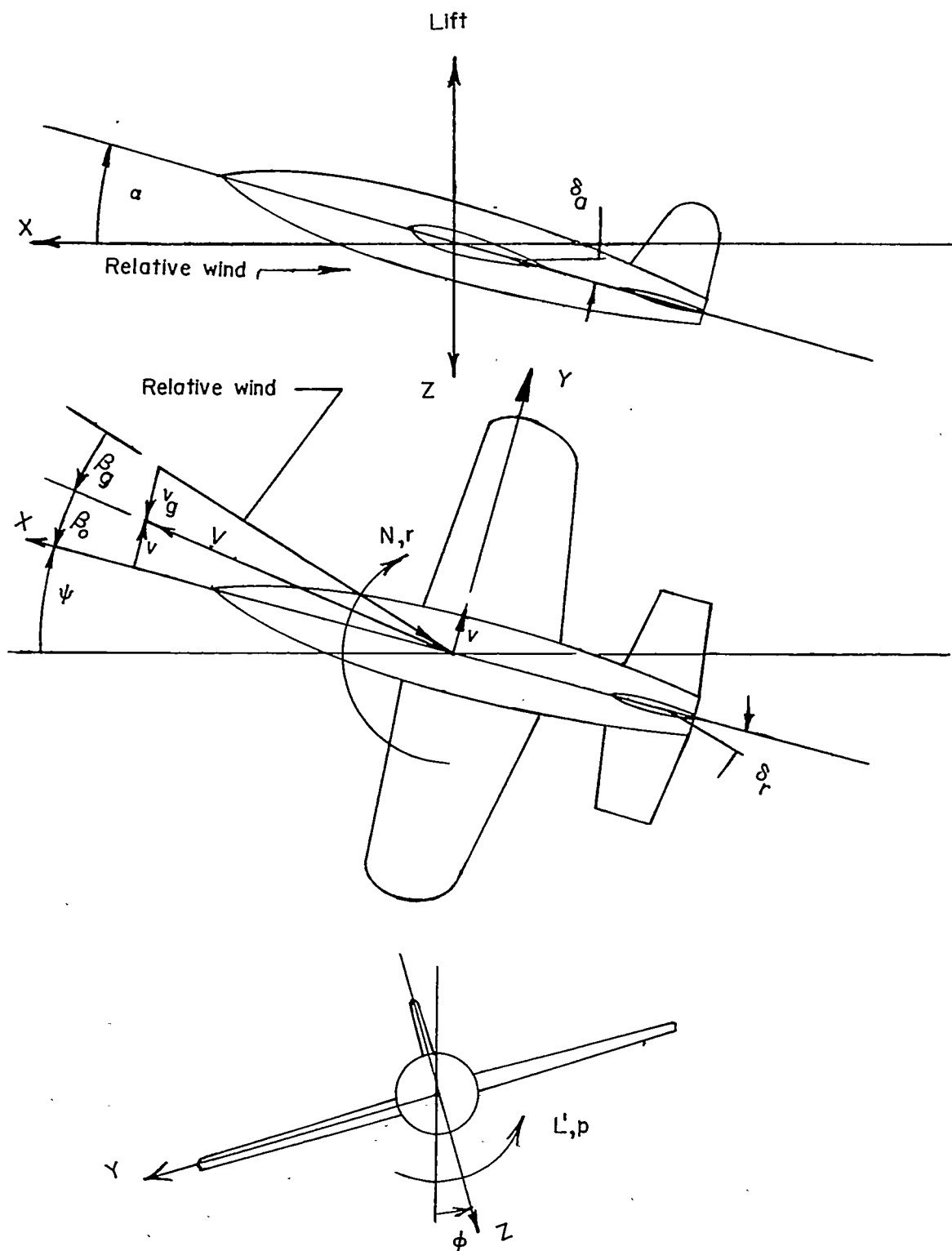


Figure 1.- Stability system of axes. Arrows indicate positive direction of forces, moments, and angular velocity. All angles are shown positive.

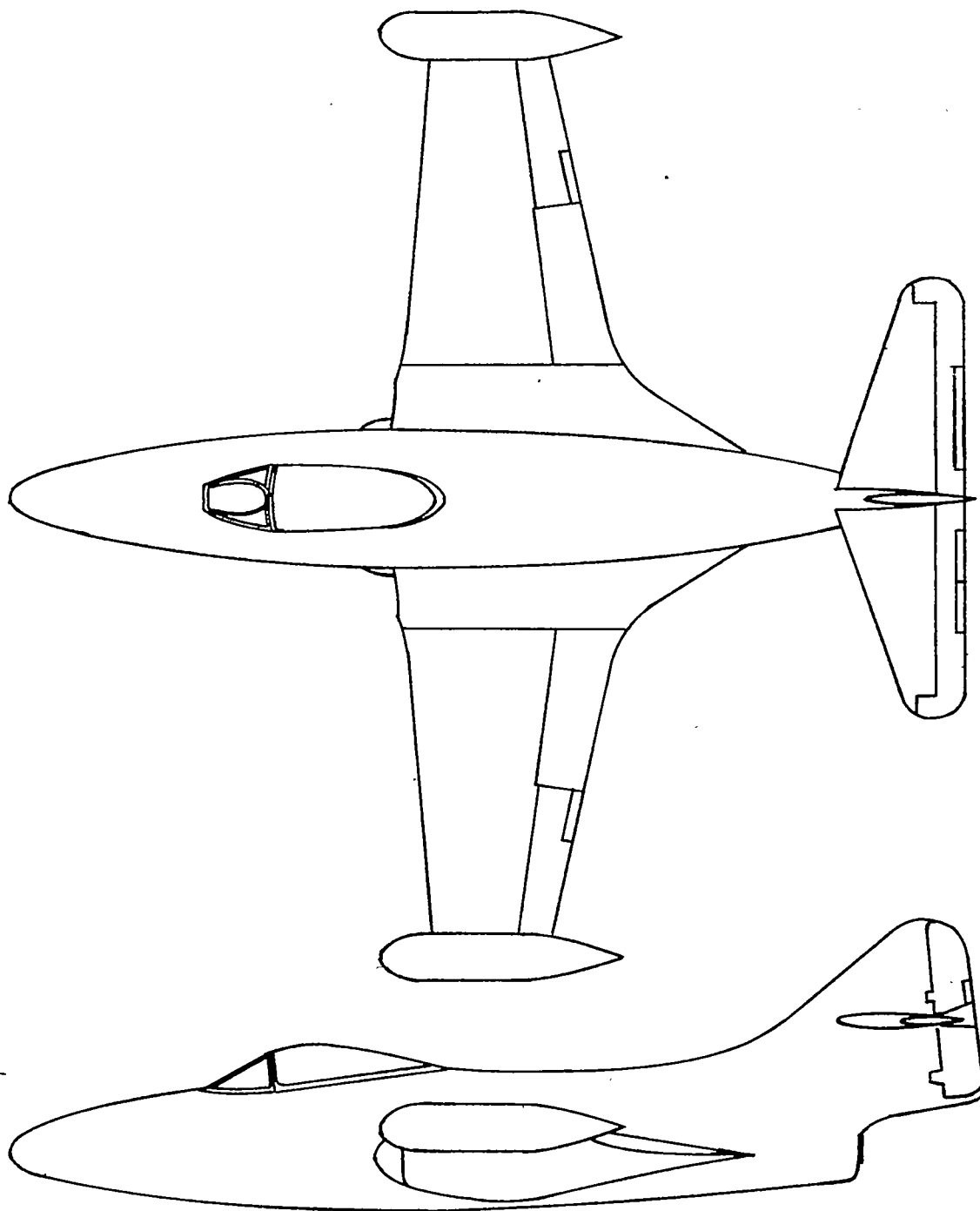


Figure 2.- Fighter airplane used in investigation.

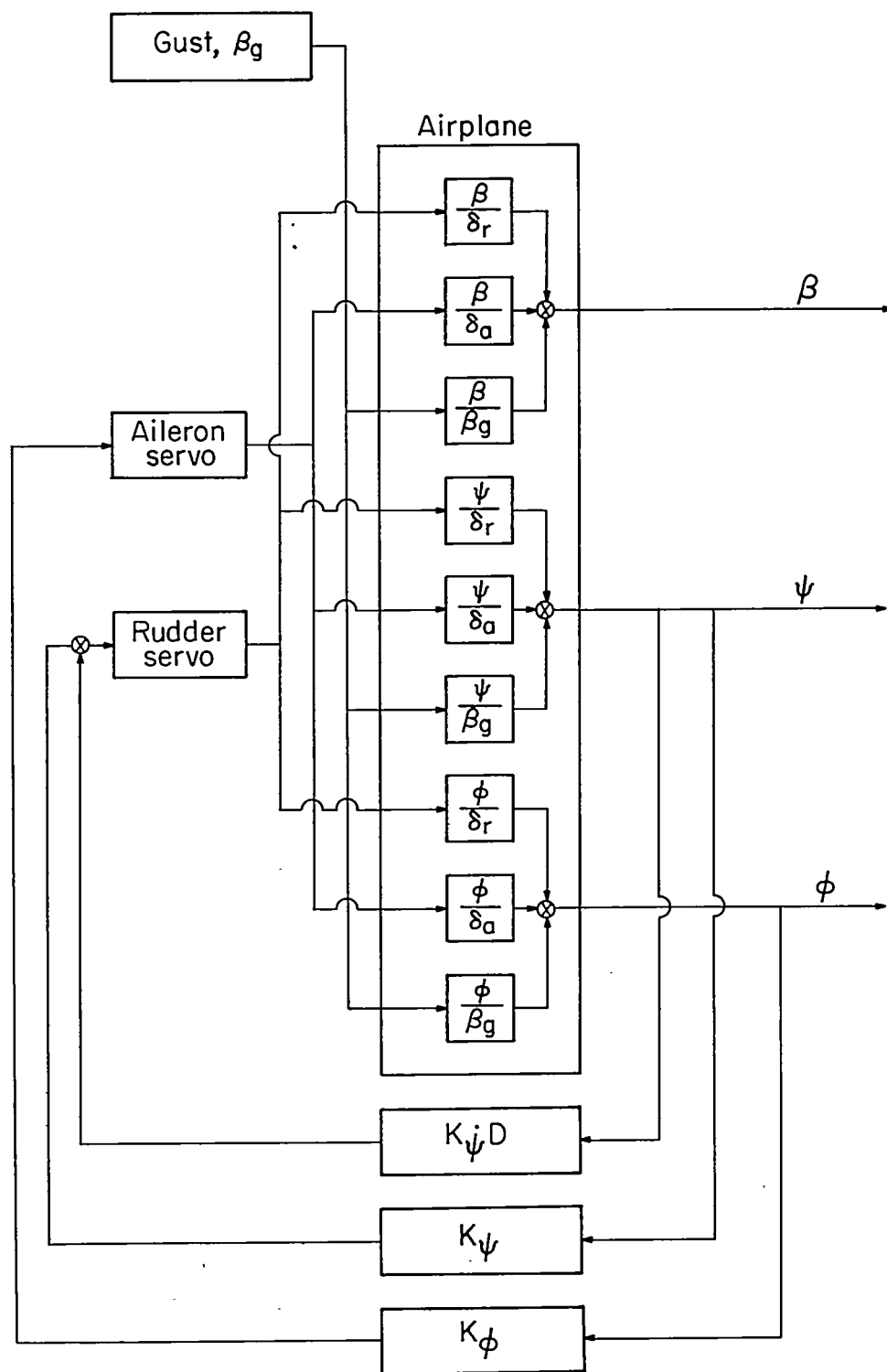


Figure 3.- Sample block diagram illustrating method of calculation of gust response of the airplane-autopilot combination.

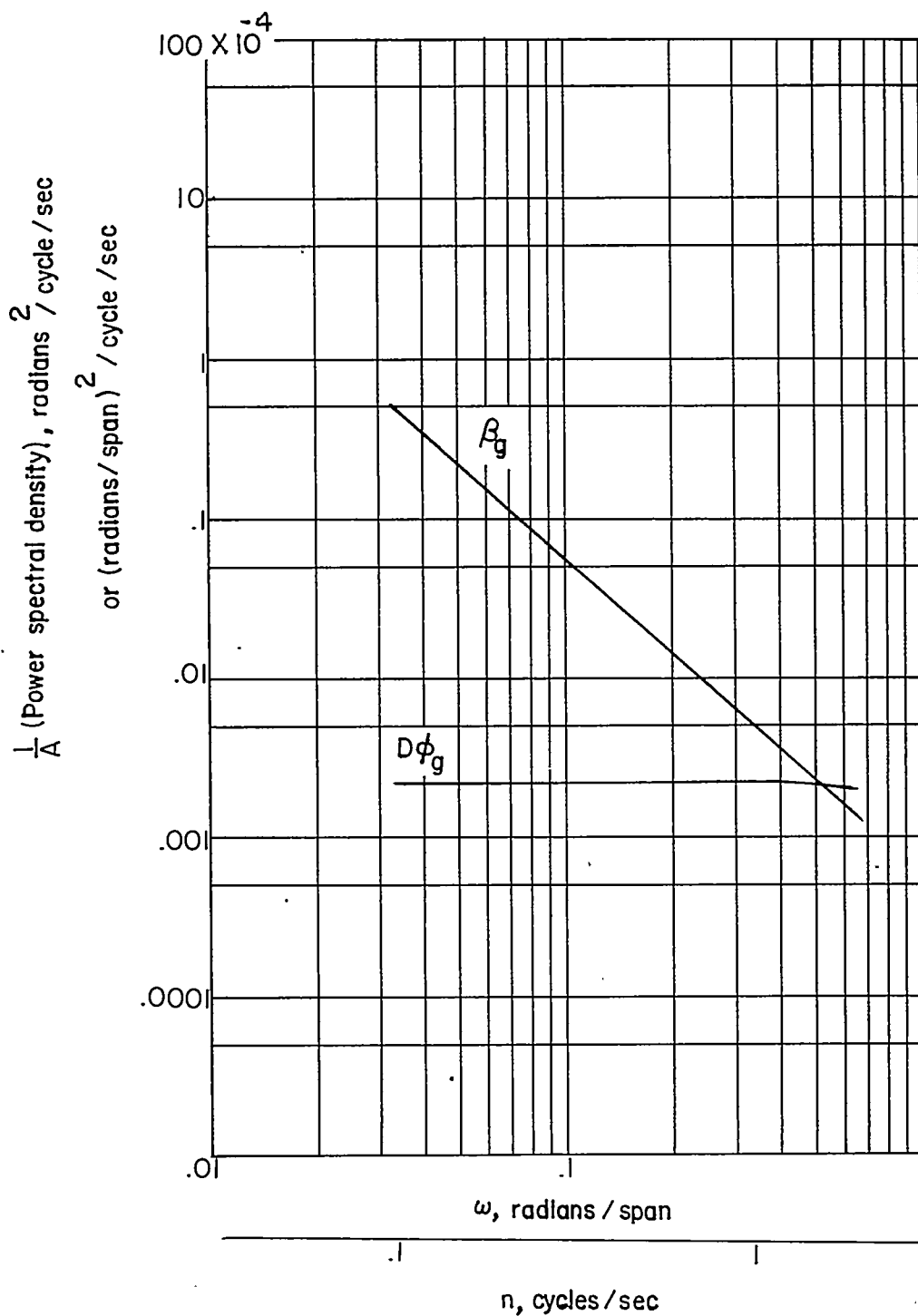
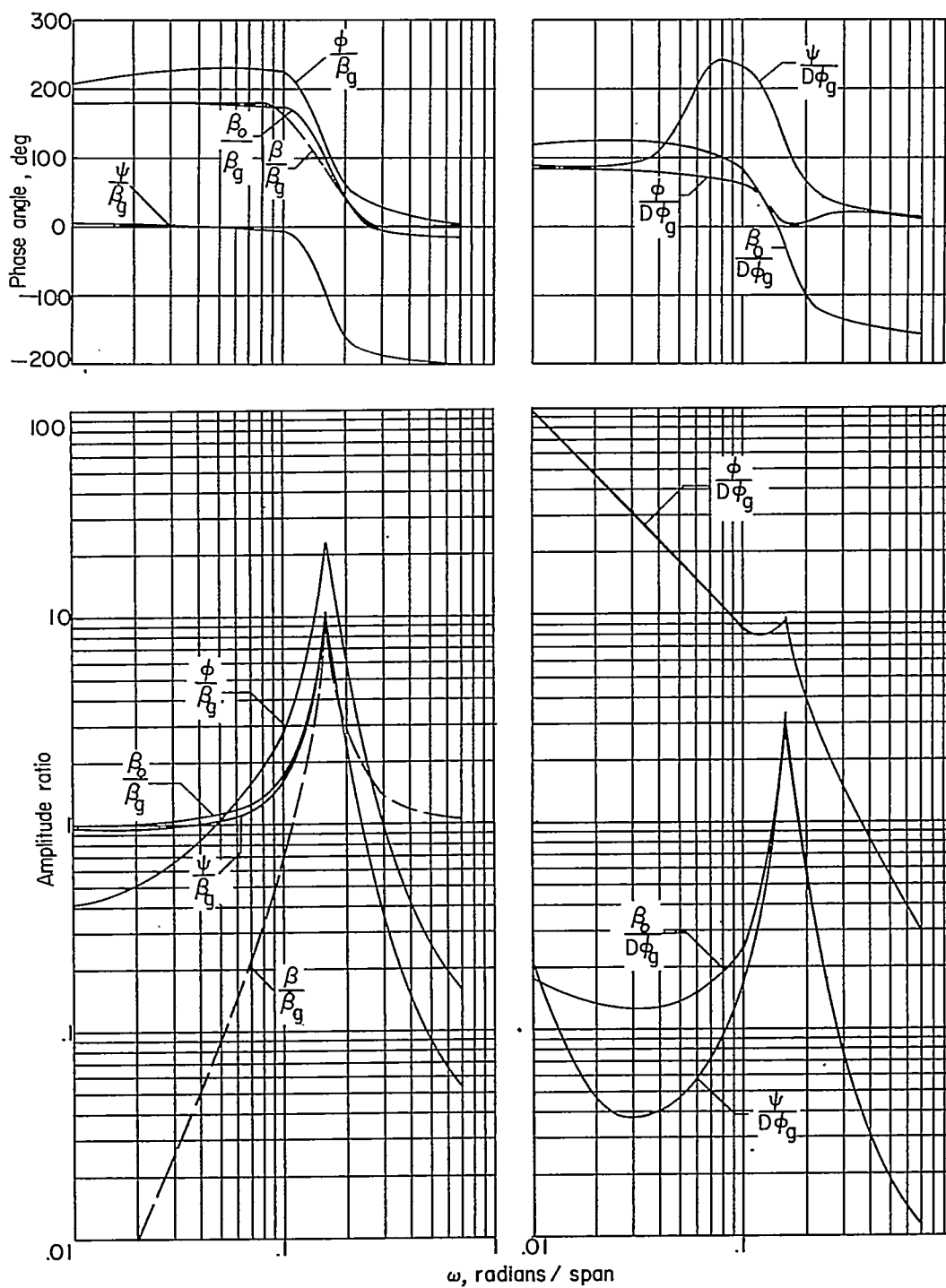


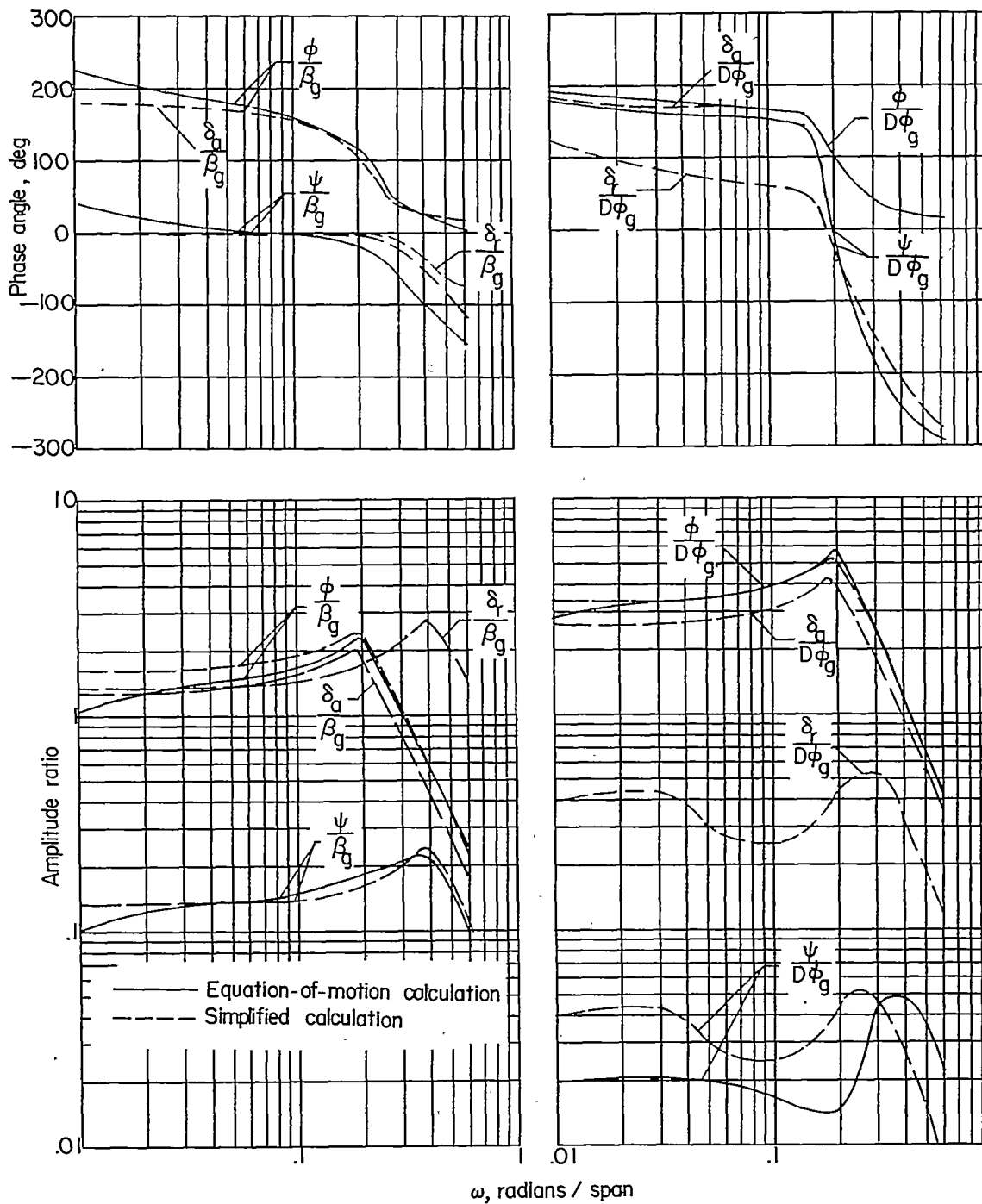
Figure 4.- Power spectral density of side gusts and rolling gusts as present in actual turbulence. (Values shown are derived from ref. 2. Constant $1/A$ is a nondimensional intensity factor which depends on altitude and meteorological conditions.)



(a) Side gusts.

(b) Rolling gusts.

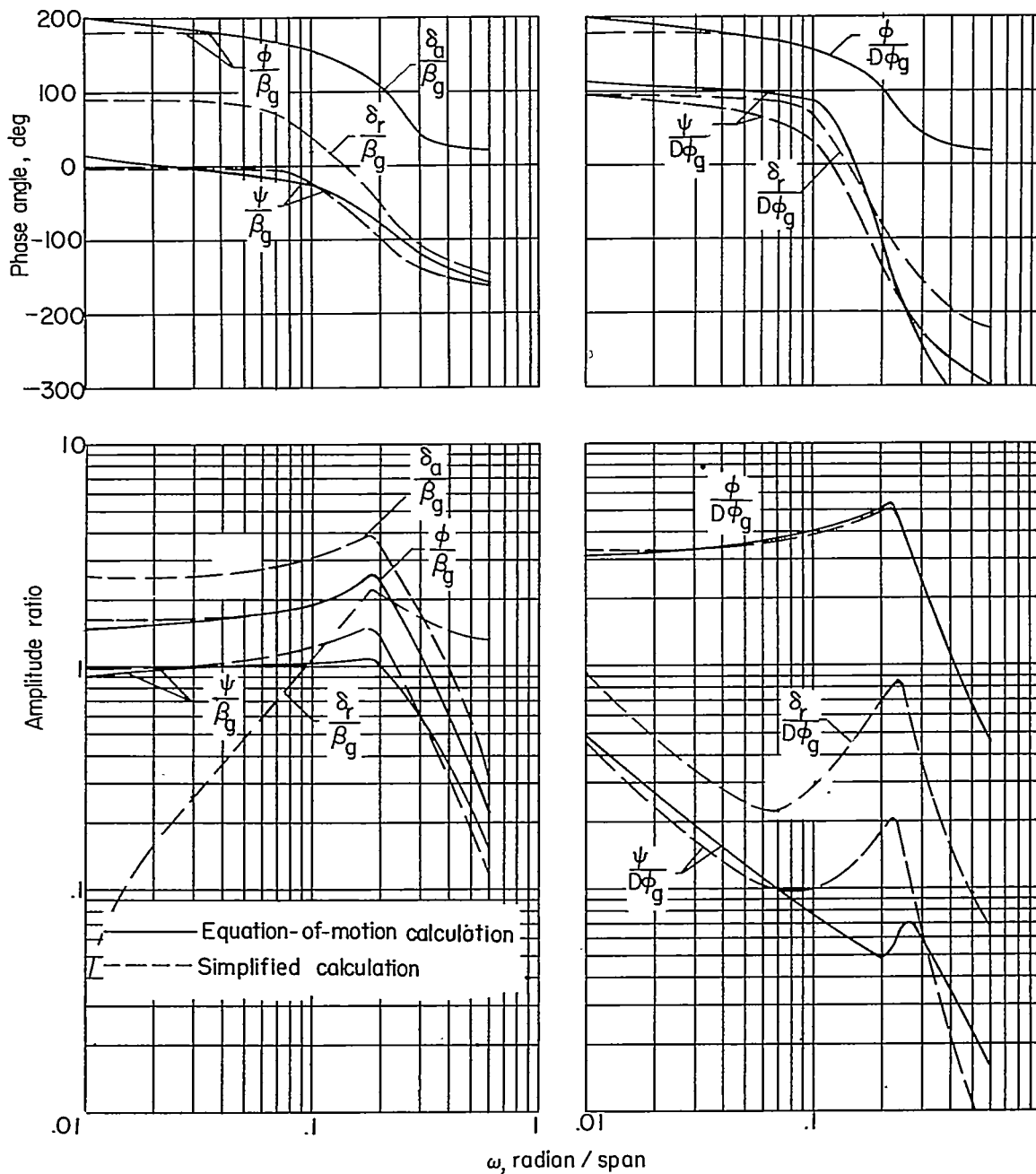
Figure 5.- Response to gusts of the airplane with controls fixed.
 $M = 0.7$; altitude, 30,000 feet.



(a) Side gusts.

(b) Rolling gusts.

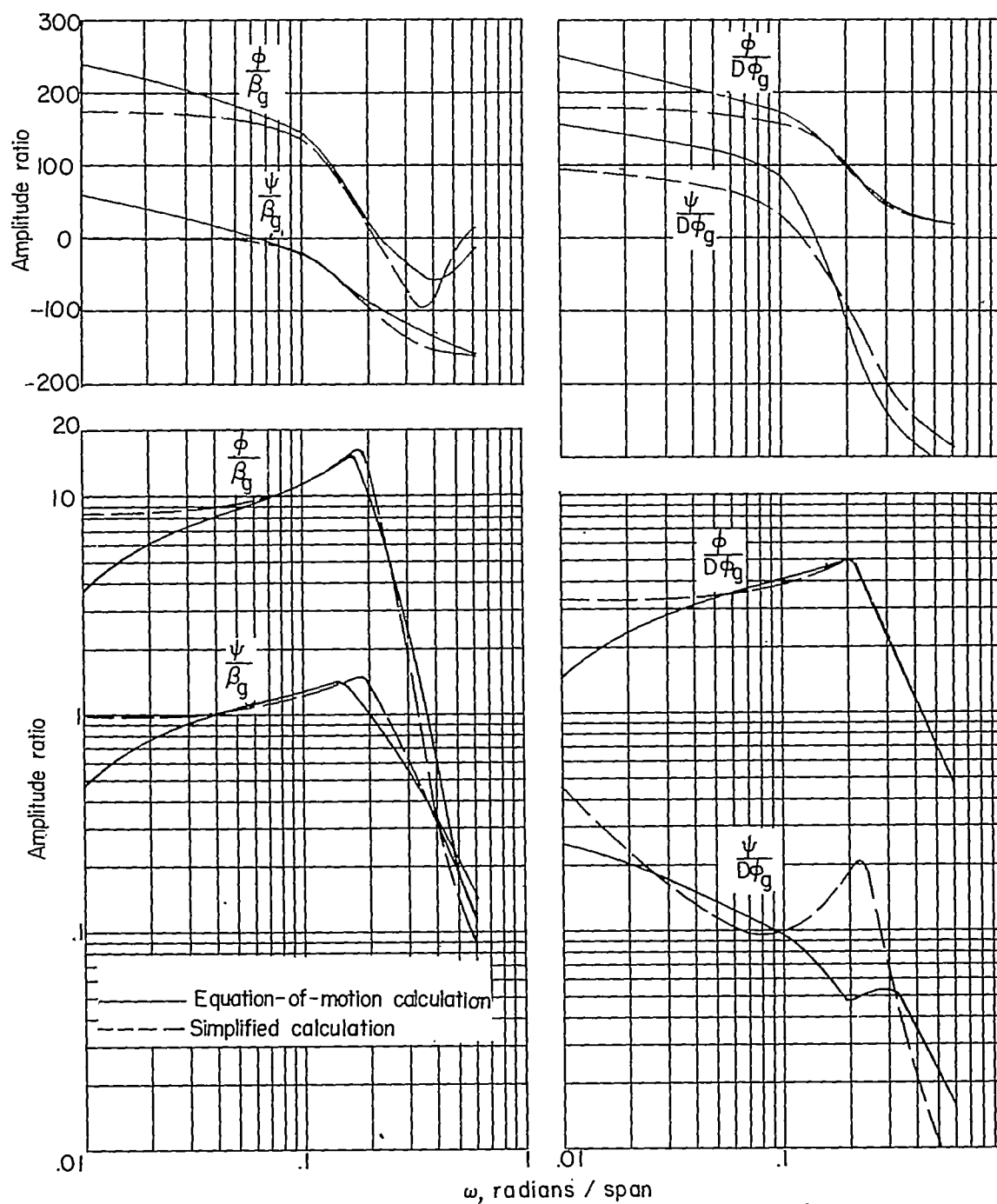
Figure 6.- Response to gusts of the airplane in combination with the type 1 autopilot. $M = 0.7$; altitude, 30,000 feet.



(a) Side gusts.

(b) Rolling gusts.

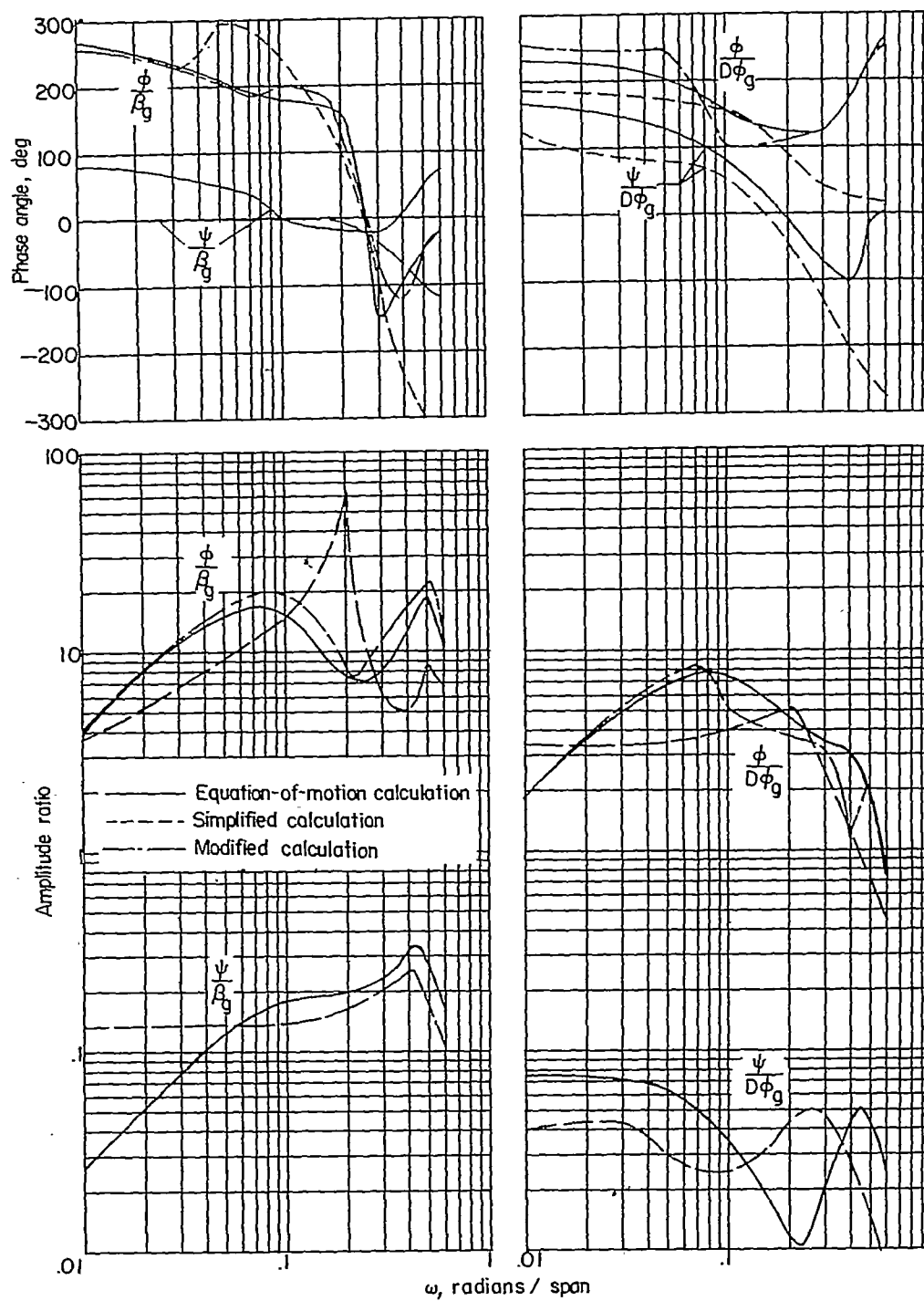
Figure 7.- Response to gusts of the airplane in combination with the type 2 autopilot. $K_\psi = 23$; $M = 0.7$; altitude, 30,000 feet.



(a) Side gusts.

(b) Rolling gusts.

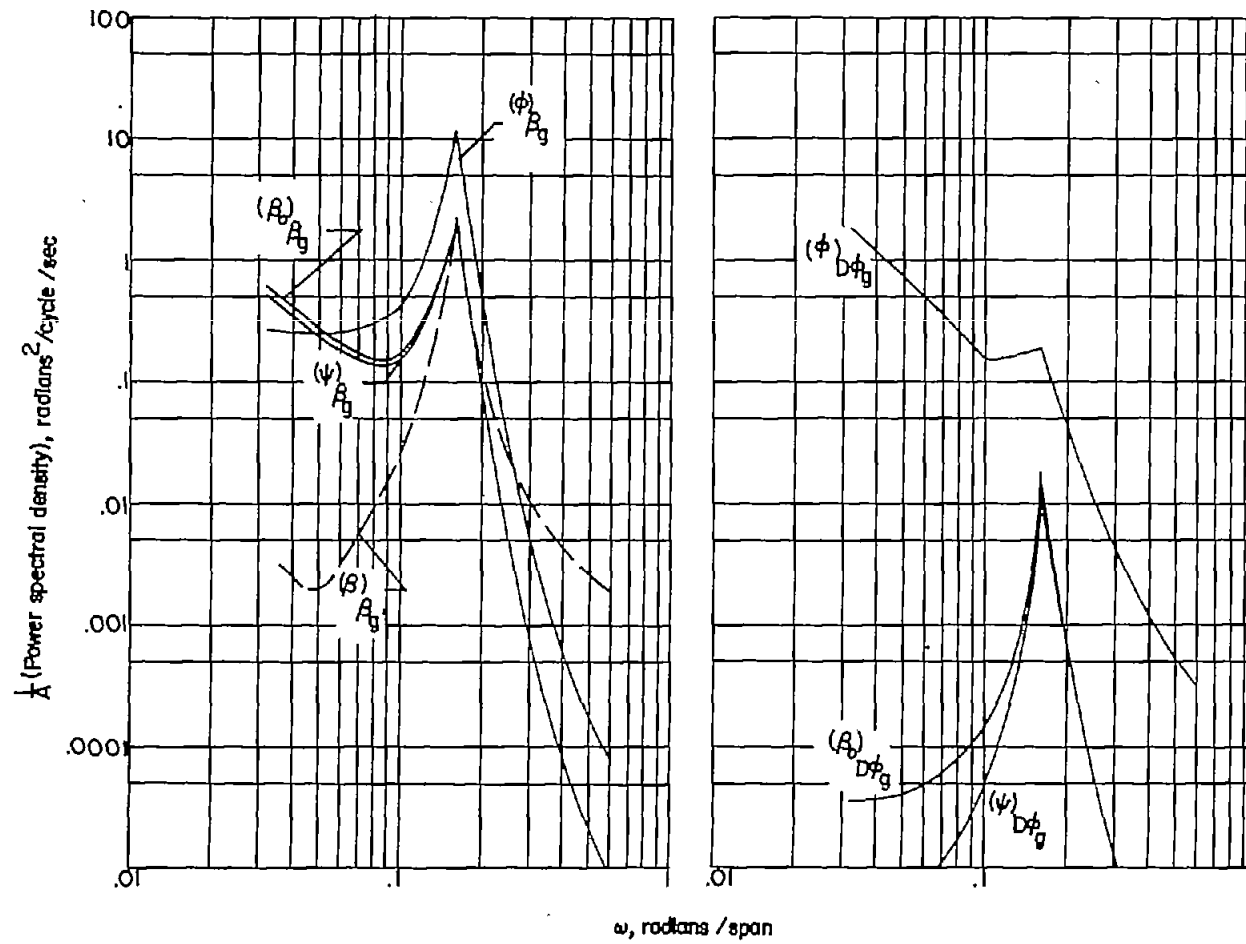
Figure 8.- Response to gusts of the airplane in combination with the type 2 autopilot. $K_v = 114$; $M = 0.7$; altitude, 30,000 feet.



(a) Side gusts.

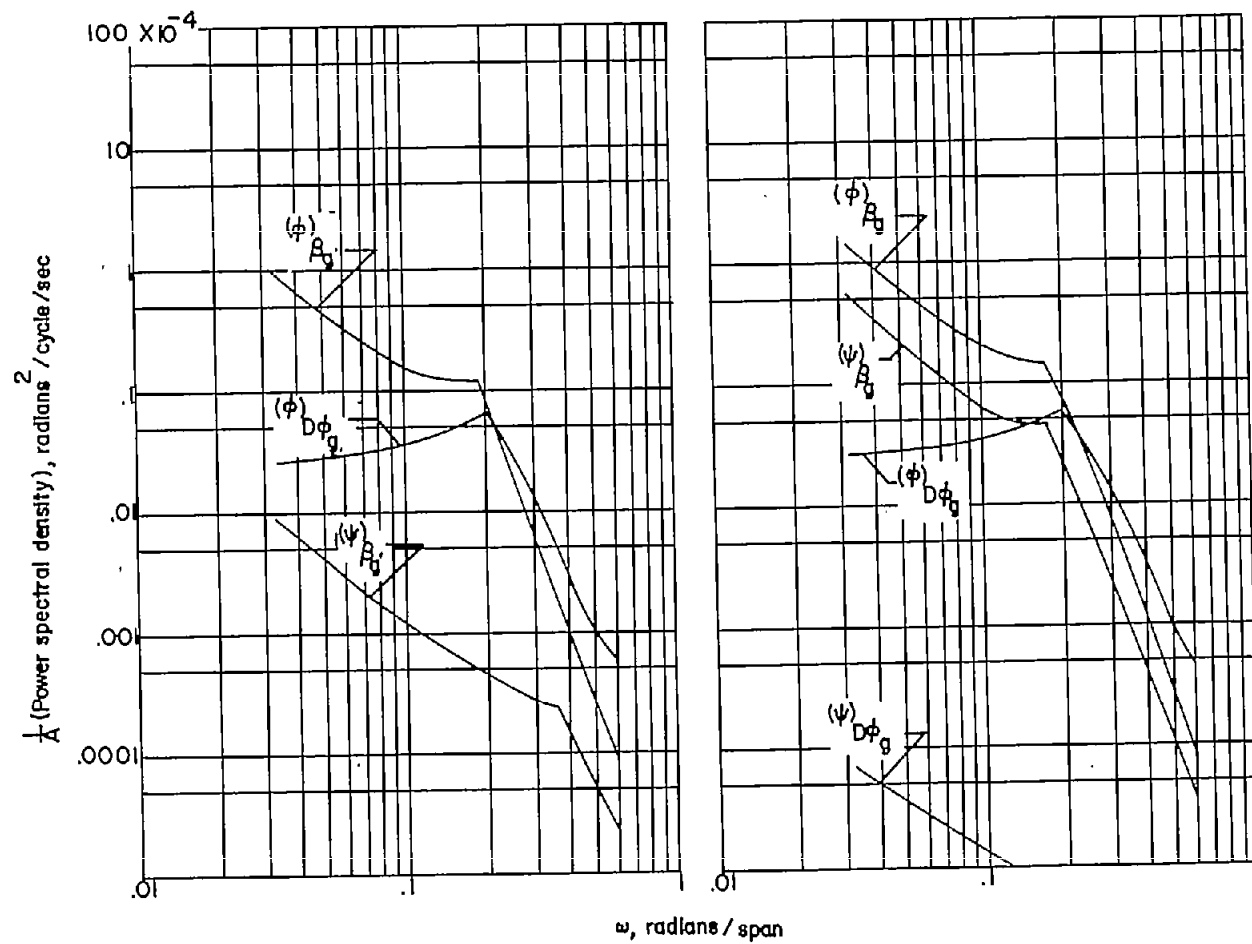
(b) Rolling gusts.

Figure 9.- Response to gusts of the airplane in combination with the type 3 autopilot. $M = 0.7$; altitude, 30,000 feet.



(a) Airplane with controls fixed.

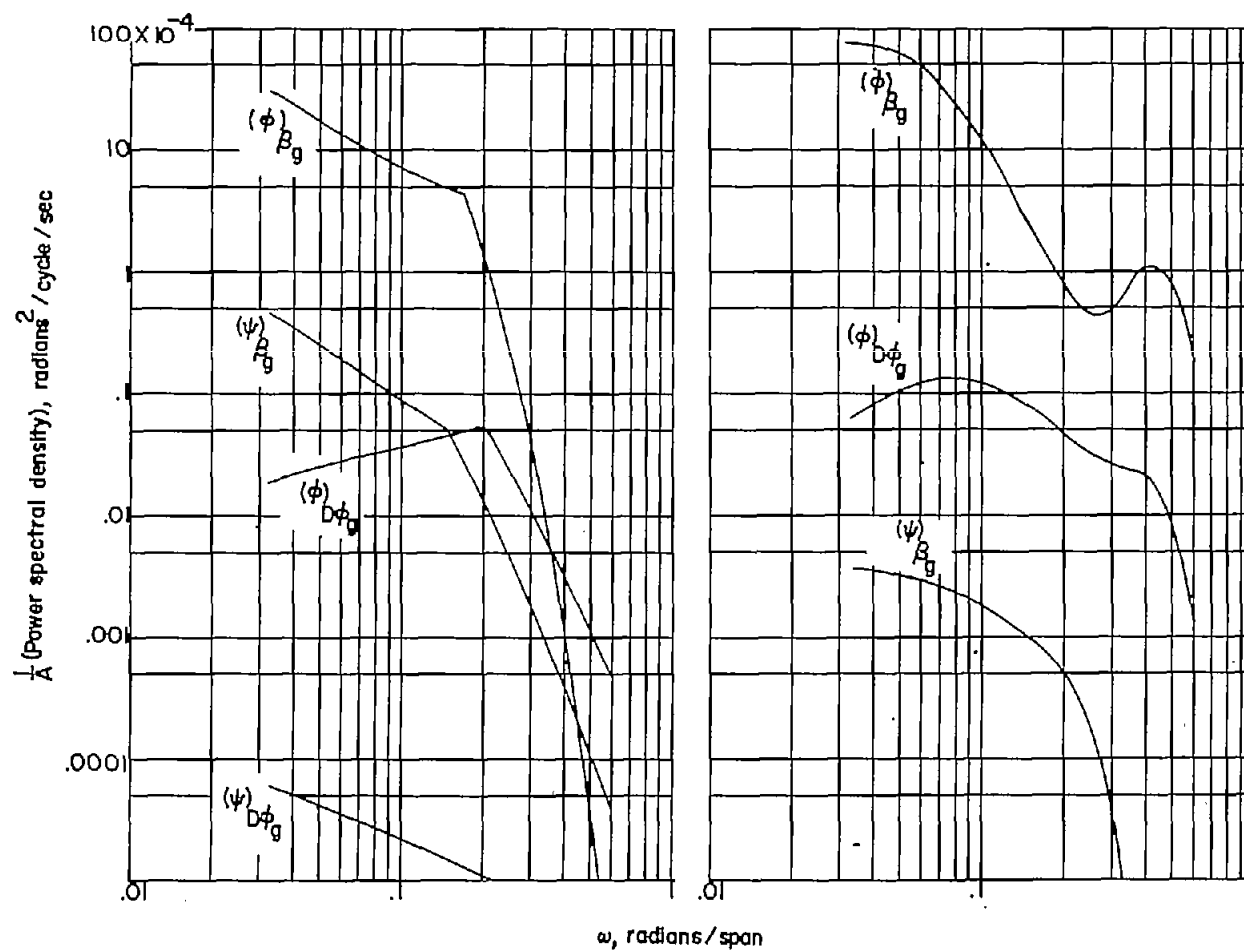
Figure 10.- Power spectral density of the motion of the airplane in response to side gusts and rolling gusts.



(b) Airplane in combination with type 1 autopilot.

(c) Airplane in combination with type 2 autopilot. $K_v = 23$.

Figure 10.- Continued.



(d) Airplane in combination with type 2 autopilot. $K_v = 114$. (e) Airplane in combination with type 3 autopilot.

Figure 10.- Concluded.

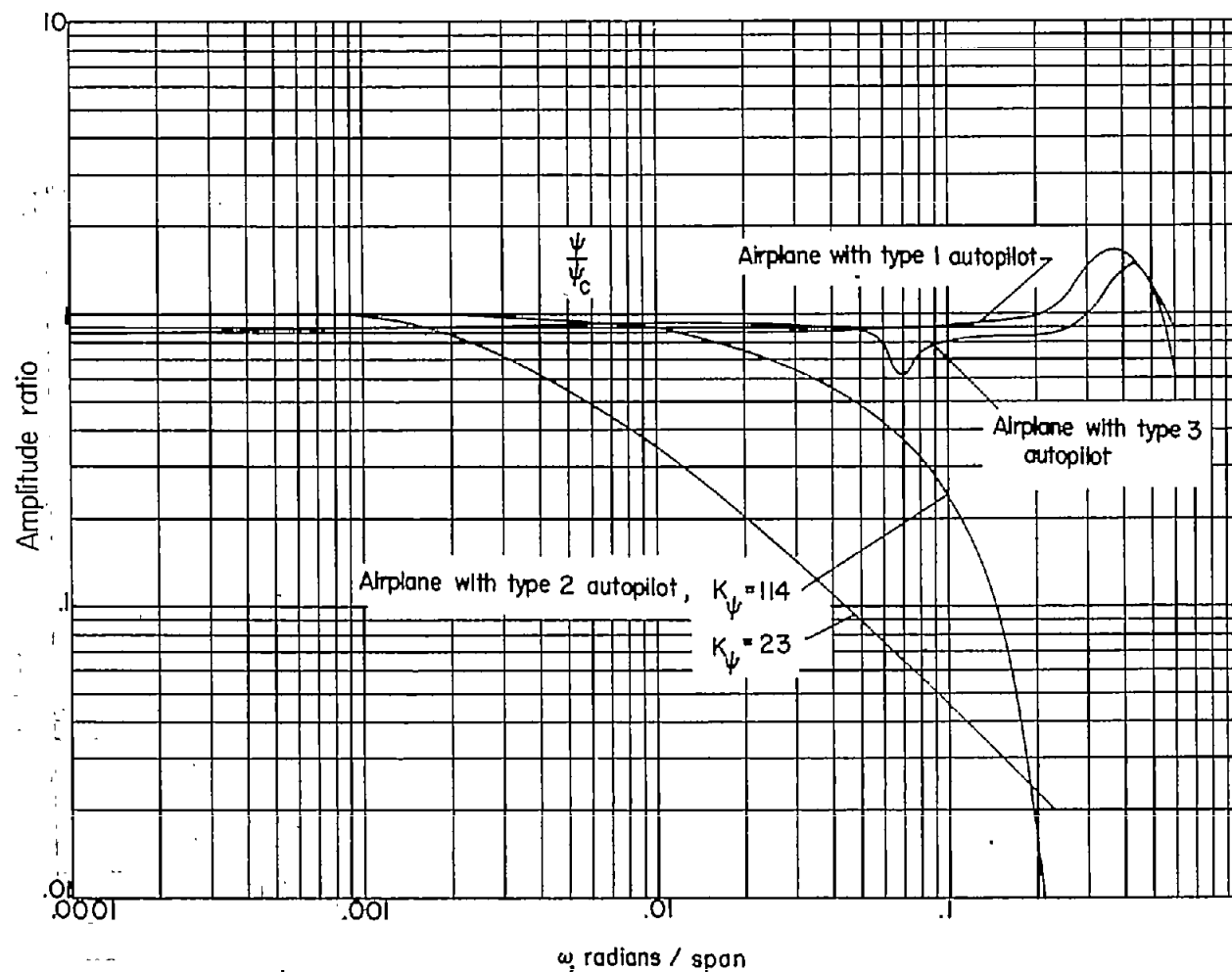


Figure 11.- Variation of heading with heading command for the airplane in combination with each of the three autopilots. $M = 0.7$; altitude, 30,000 feet.

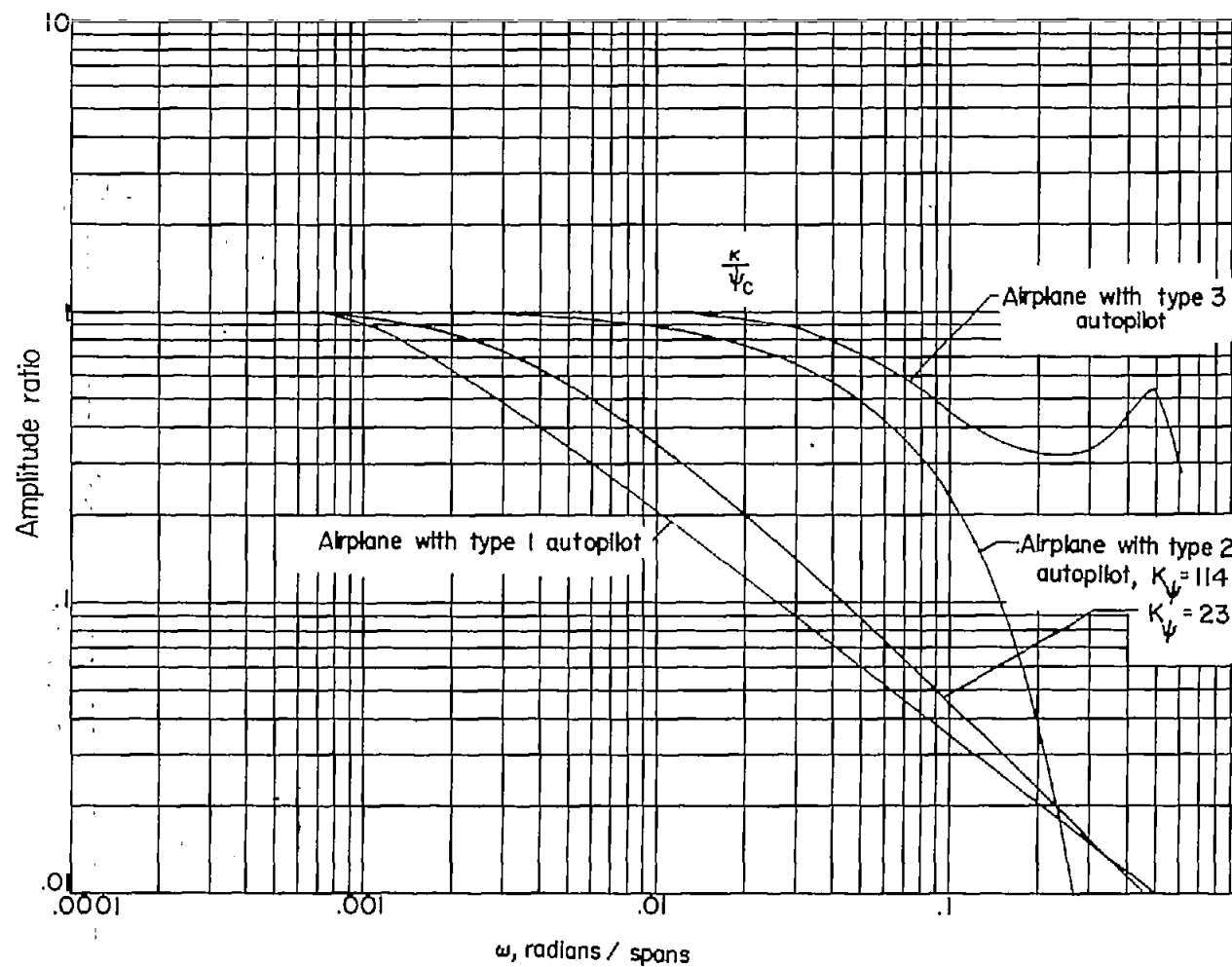
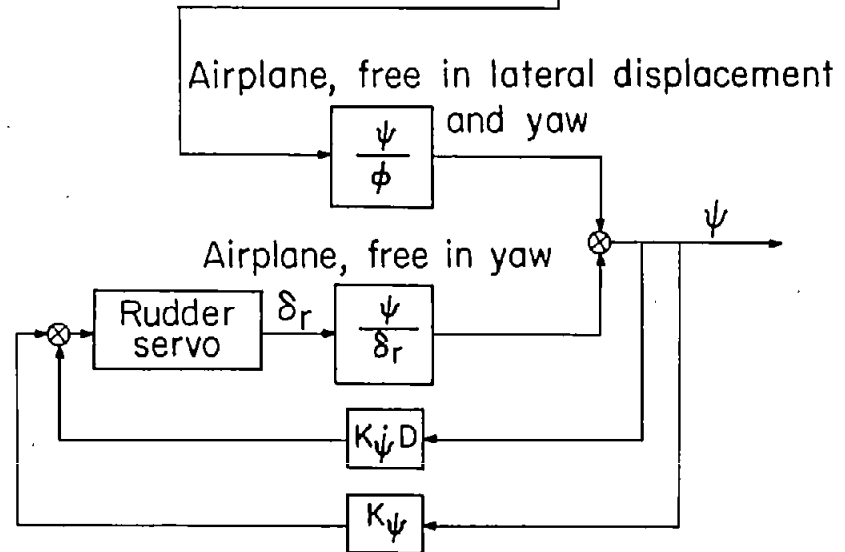
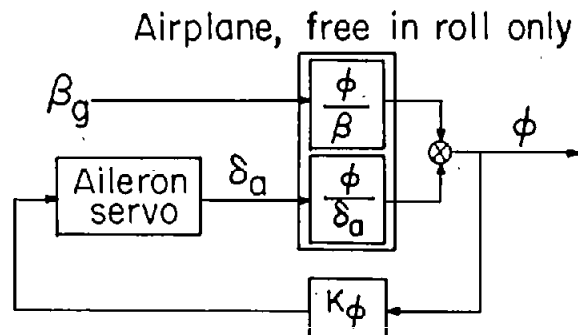
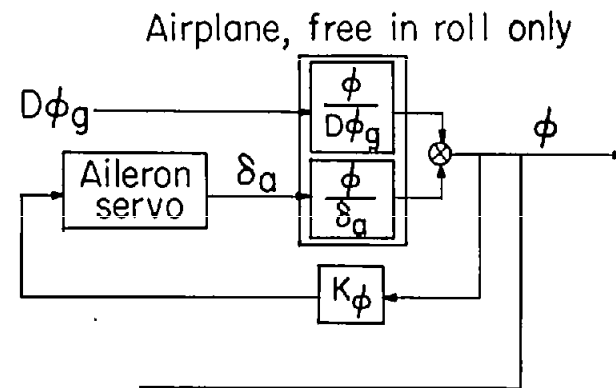
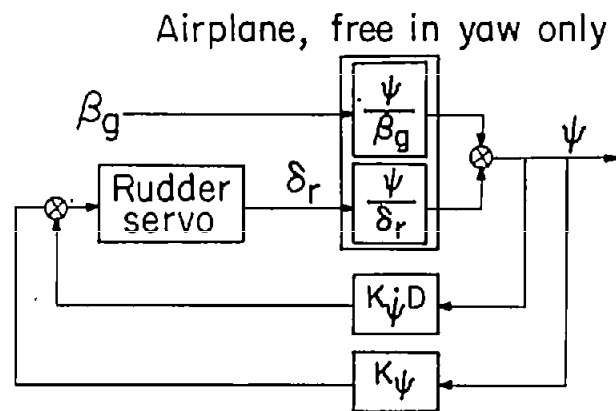


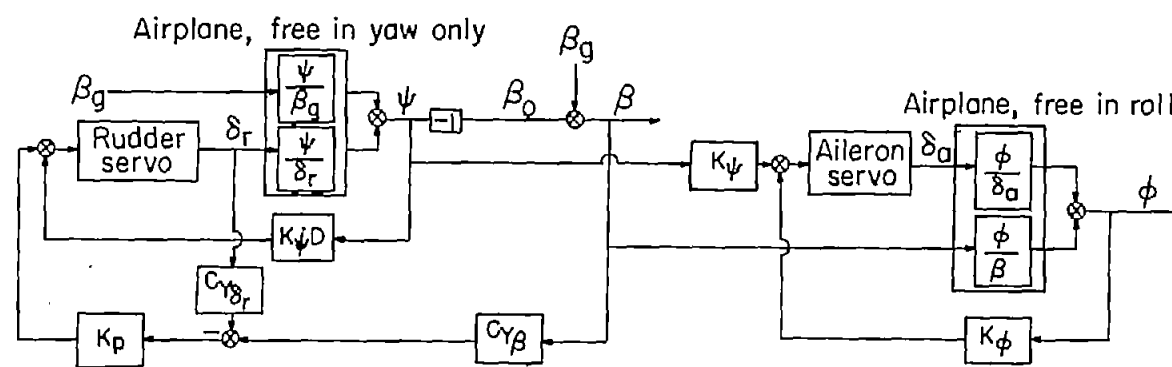
Figure 12.- Variation of course with heading command for the airplane in combination with the three autopilots. $M = 0.7$; altitude, 30,000 feet.



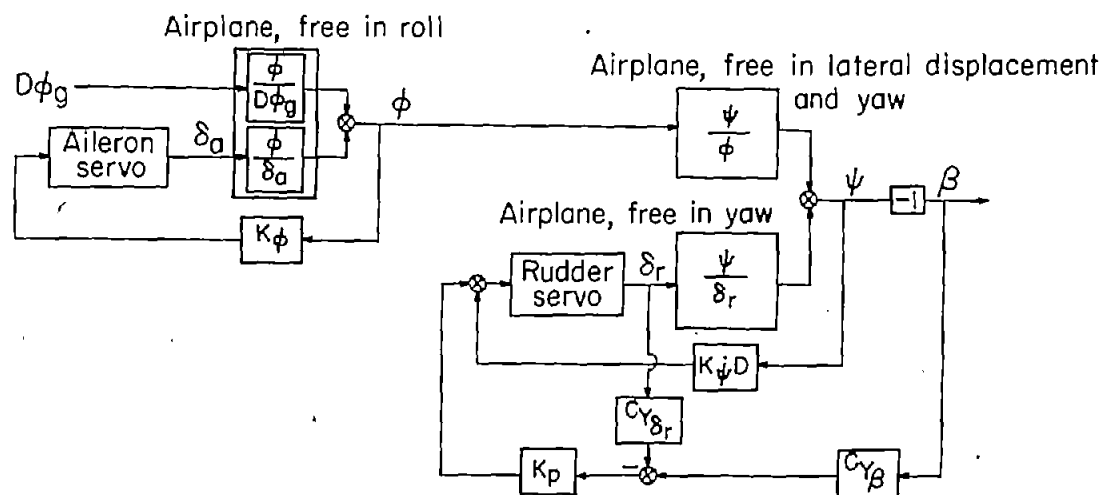
(a) Side gusts.

(b) Rolling gusts.

Figure 13.- Simplified transfer-function method of calculating gust response of airplane in combination with type 1 autopilot.

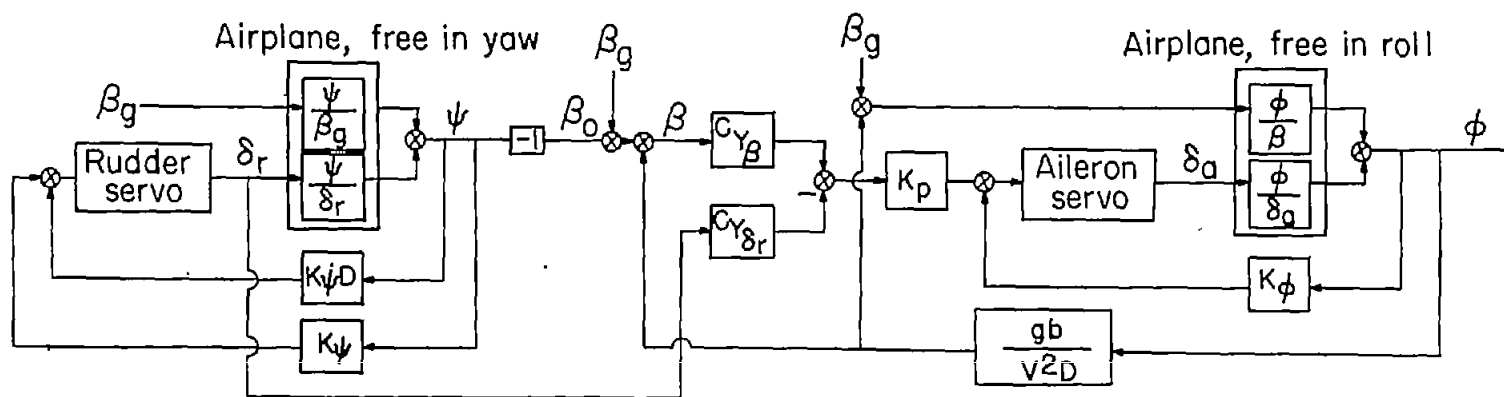


(a) Side gusts.

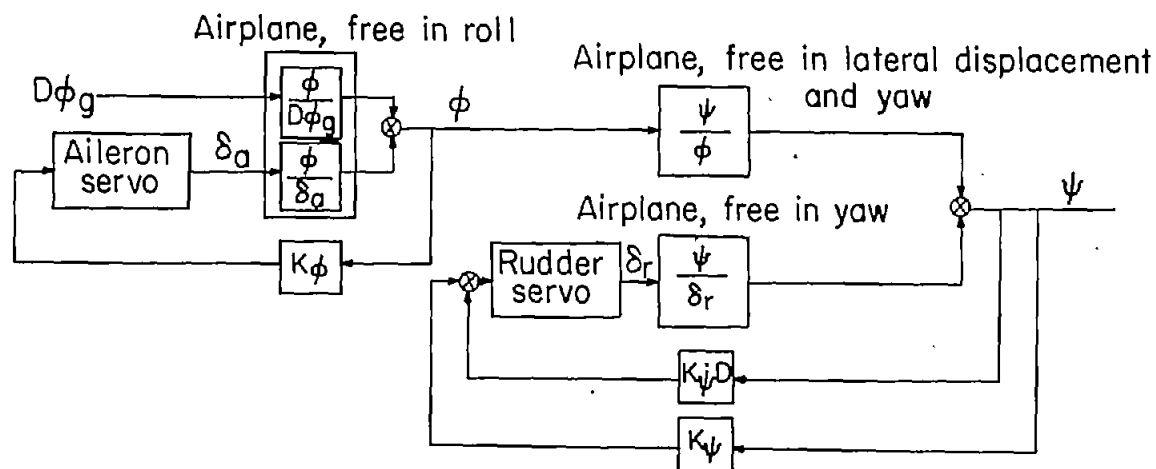


(b) Rolling gusts.

Figure 14.- Simplified transfer-function method of calculating gust response of airplane in combination with type 2 autopilot.



(a) Side gusts.



(b) Rolling gusts.

Figure 15.- Simplified transfer-function method of calculating gust response of airplane in combination with type 3 autopilot.